Ultraviolet-based heterogeneous advanced oxidation processes as technologies to remove pharmaceuticals from wastewater: An overview

J. Meijide [a,b,*], G. Lama [a], M. Pazos [a], M.A. Sanromán [a], P.S.M. Dunlop [b]

[a] CINTECX, Universidade de Vigo, BIOSUV Group, Campus Lagoas-Marcosende, Vigo, 36310, Spain
[b] Nanotechnology and Integrated BioEngineering Centre, School of Engineering, University of Ulster, Newtownabbey BT37 0QB, United Kingdom

ARTICLE INFO

ABSTRACT

Contaminants of emerging concern including pharmaceuticals and personal care products are increasingly detected at low concentrations in surface waters. Given the associated toxicity of these compounds, there is the potential for significant impacts on aquatic life and the food chain. Since most pharmaceuticals are not biodegradable, they cannot be removed by secondary treatment processes in conventional wastewater treatment plants. Therefore, the development of alternative treatment methods plays a critical role in the removal of pharmaceuticals. Energy consumption is a key factor in technology selection, and the use of solar energy may help minimise operating costs. Thus, this work provides a comprehensive review of relevant research published between 2016 and 2021 targeting the removal of active pharmaceutical ingredients using ultraviolet processes, including photo-Fenton, photocatalysis and photoelectrocatalysis. While the focus remains on the development of novel catalysts and some efforts have been made to demonstrate the reuse of these materials for multiple cycles, there is little work aimed at scaling up the systems or investigating their efficacy in real water matrices to test the potential beyond the laboratory setting. The review concludes with some recommendations for future studies, highlighting the importance of comparing technologies in terms of life cycle assessment, energy use, and financial considerations to provide a holistic understanding of the role that these technologies can play in removing trace pharmaceutical compounds from wastewater.

1. Introduction

The negative effects of the use of pharmaceuticals in human and veterinary medicine on the environment have been reported by the scientific community [1,2]. Improper use significantly increases the compound concentration in receiving waters, resulting in toxic and mutagenic effects and contributing significantly to the development of antimicrobial resistance, where bacteria in human and animal hosts are no longer treatable with antibiotics. After administration, pharmaceutical residues are excreted in the urine and faeces as biologically active, unchanged parent molecules, metabolites, and/or conjugates [3]. Major sources of residues entering the aquatic environment through wastewater treatment plants include domestic sewage, hospitals, the pharmaceutical industry and inappropriate disposal of expired drugs. The ubiquitous presence of pharmaceuticals in the environment has been demonstrated by their presence in every environmental matrix studied, including surface water, groundwater, soil, sludge, and sediment samples. Due to the recalcitrant nature and inherent biological stability of

both the parent compound and metabolites, conventional secondary wastewater treatment systems cannot completely remove trace compounds. Fluoroquinolones, sulphonamides, tetracyclines and β-blockers have removal efficiencies of 40–75%, while non-steroidal anti-inflammatory drugs (NSAIDs) generally have higher removal efficiencies of about 90%, with the exception of diclofenac (below 60%). Therefore, alternative technologies are needed to further reduce the risk of transfer of these micropollutants to the aquatic environment [4].

To improve removal efficiency, conventional wastewater treatment plants (WWTPs) require additional support and technologies to further reduce the risk of transferring these micropollutants to the aquatic environment. Ultraviolet (UV)-based oxidation processes have the ability to catalyse the degradation and further mineralisation of organic pollutants through the production of highly reactive radicals [5], with the potential to utilise solar energy or novel engineering solutions based on efficient LED technology. Although there is significant academic interest in this approach, further development, optimisation, and scaling of these promising approaches is needed to remove non-biodegradable

compounds commonly found in wastewater. Photo-driven chemical processes such as photo-Fenton, photocatalysis, and photo-electrocatalysis rely on UV irradiation and strong oxidants, e.g., hydrogen peroxide, or iron- and titanium dioxide-based catalysts to generate radical species responsible for pollutant degradation. These environmentally friendly technologies are easy to operate with minimal manual effort. However, high turbidity levels resulting from the presence of natural organic matter, inorganic materials, and biological organisms can cause significant problems due to fouling and light scattering [6]. For most advanced oxidation processes, pre-filtration with 5–20-micron filters is strongly recommended prior to UV-treatment.

Previous laboratory scale studies using direct UV-C treatment have shown that several antibiotics are not completely removed from aqueous solutions [7]. In addition, bacterial regrowth may occur during water storage, which promotes the persistence of antibiotic-resistant bacteria. Therefore, combining the effects of photolysis and catalysis offers synergistic advantages, and the choice of UV source is critical. Most stable semiconductors used as photocatalysts, have a band gap corresponding to energy in the ultraviolet region ($E_{bg} \geq 3.2$ eV); therefore, these materials respond to the photocatalytic process when exposed only to ultraviolet radiation. Usually, UV sources are tuned to the classical ranges UV-C: 200–280 nm; UV-B: 280–315 nm; UV-A: 315–400 nm (for comparison, visible light ranges from 400 to 760 nm). However, special narrow-band multi-frequency approaches can also be used by combining lamps and light-emitting diodes.
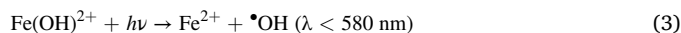
Various lamp types have been successfully used for UV-based advanced oxidation technologies, including carbon arc, metal halide, xenon arc, mercury-xenon, tungsten-halogen, high-pressure sodium vapour, argon arc, and light-emitting diode lamps (LEDs) [8]. Recently, UV-LEDs have attracted special interest in wastewater treatment due to their environmentally friendly materials and production techniques, high photonic performance and long lifetime. Considering that electricity is converted into photons with high efficiency (about 90%), much less energy is required to produce a similar UV flux compared to conventional lamps. Given the high cost of UV-C LED and the complexity of efficiently removing heat from sources, the use of conventional light sources continues to be widely reported in the literature over the past five years. A wide range of solar simulation sources that mimic the full spectrum of UV, visible and IR wavelengths are also commonly used for laboratory research [9].

According to the Scopus® database, approximately 15,000 articles (reviews, reports, data studies, and books) have been published in the last 5 years, specifically related to the use of UV-radiation to remove drug compounds from wastewater. Despite the publication of several general reviews addressing the removal of pharmaceuticals, there has not been a comprehensive review of the advances and challenges associated with the use of UV-based processes to remove these specific emerging contaminants. Therefore, the goal of this work is to provide a comprehensive overview of research in this area from 2016 to 2021 and develop recommendations to help the community fill knowledge gaps in this advancing area of research.

2. Heterogeneous photo-Fenton process

The Fenton process is a powerful oxidation-based technology, which effectively degrades contaminants via a series of biodegradable intermediates, resulting in near-complete mineralisation (Fig. 1). Enhancement of the Fenton reaction (Eq. (1)) can occur through the absorption of long and short wavelength radiation, which generates additional hydroxyl radicals through two key processes (a) regeneration of iron ions through the formation of iron complexes under acidic conditions (Eqs. (2) and (3)) and (b) photolysis of hydrogen peroxide (Eq. (4)) [10].

$$Fe^{2+} + H_2O_2 \rightarrow Fe^{3+} + {}^{\bullet}OH + OH^- \tag{1}$$

$$Fe^{3+} + H_2O \rightarrow Fe(OH)^{2+} + H^+ \tag{2}$$

$$Fe(OH)^{2+} + h\nu \rightarrow Fe^{2+} + {}^{\bullet}OH \ (\lambda < 580 \text{ nm}) \tag{3}$$

$$H_2O_2 + h\nu \rightarrow 2\ {}^{\bullet}OH \ (\lambda < 310 \text{ nm}) \tag{4}$$

Despite the potential to use solar energy to drive the process, photo-Fenton is dependent on the supply of consumable chemicals, which could hinder widespread industrial use. For this reason, several strategies have been proposed to minimise operating costs but also to improve efficiency by introducing heterogeneous catalysts and/or chelating agents [11]. Relevant publications dealing with drug mineralisation by heterogeneous photo-Fenton processes are summarised in Table 1.

2.1. Materials used as heterogeneous photo-Fenton

Considerable academic efforts continue to focus on the development of novel materials. Iron-based oxides are extensively applied as heterogeneous photo-Fenton catalysts due to their low cost, negligible toxicity, efficient charge separation properties, and easy recovery [11, 12]. The base semiconductor can be excited by radiation to produce photogenerated electrons via a multistep mechanism described by Eqs. (5)–(11) [13,14].
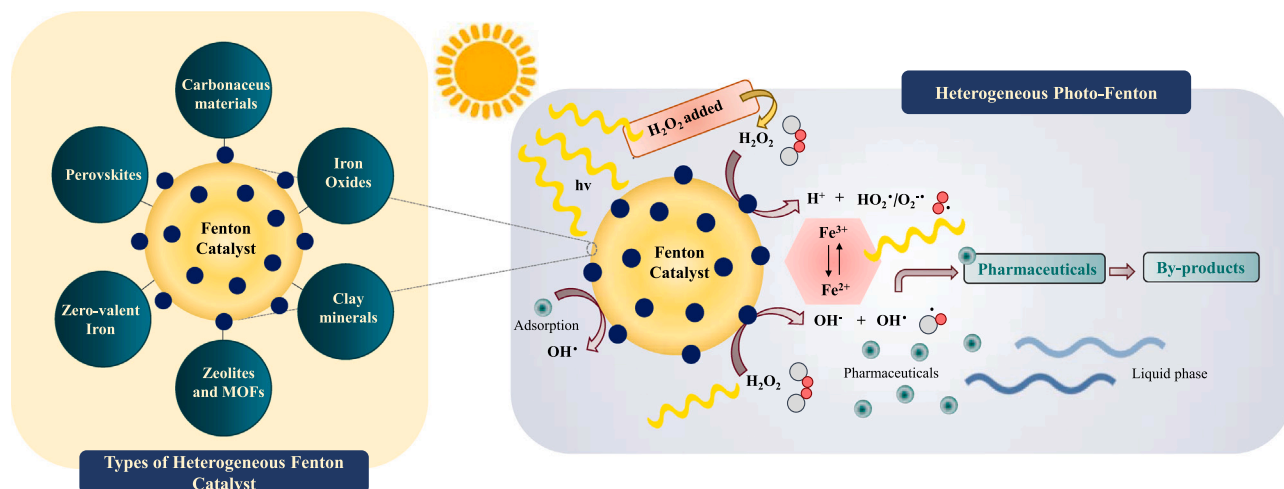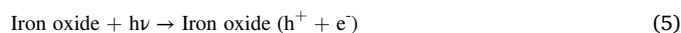
$$\text{Iron oxide} + h\nu \rightarrow \text{Iron oxide } (h^+ + e^-) \tag{5}$$

Fig. 1. Photo-Fenton mechanism.

Table 1

Summary of some relevant studies on heterogeneous photo-Fenton systems.

| Pharmaceutical (concentration)	Catalyst (concentration)	Light source	Operational conditions	Removal and TOC decay	Ref.
Paracetamol (15 mg/L)	α-FeOOH (1 g/L)	Low pressure Hg lamps (λ = 365 nm)	$[H_2O_2]_0$ = 5 mM, pH= 5.9	45% removal (180 min)	[15]
Sulfamethoxazole (10 mg/L)	$CuFe_2O_4$ (0.2 g/L)	300 W Xe lamp (λ = 420 nm)	$[H_2O_2]_0$ = 10 mM, pH= 6.73	96% removal (120 min) 31% TOC decay (120 min)	[16]
Ciprofloxacin/carbamazepine (5 mg/L TOC)	$MnFe_2O_4$ (n.a.)	500 W LED lamp (solar simulator)	$[H_2O_2]/COD$ = 4.25, $[H_2O_2]/[Fe, Mn]$ = 5	95% ciprofloxacin and 25% carbamazepine removal (120 min)	[17]
Tetracycline hydrochloride (40 mg/L)	$MnFe_2O_4$/biochar (0.5 g/L)	300 W Xe lamp (λ = 420 nm)	$[H_2O_2]_0$ = 100 mM, pH= 5.5	95% removal (120 min)	[18]
Tetracycline hydrochloride (60 mg/L)	$ZnFe_2O_4$ (yolk-shell structure) (0.3 g/L)	LED lamp	$[H_2O_2]_0$ = 20 mM, pH= 6	73.6% removal (40 min)	[19]
Tetracycline hydrochloride (10 mg/L)	α-FeOOH/γ-Fe_2O_3 (0.5 g/L)	300 W Xe lamp (λ > 420 nm)	$[H_2O_2]_0$ = 10 mM, pH= 6	93% removal (60 min) 64% TOC decay (60 min)	[20]
Tetracycline hydrochloride (100 mg/L)	15% $yCeO_2$/FH (0.4 g/L)	5 W LED lamp	$[H_2O_2]_0$ = 50 mM, pH= 4	98.7% removal (60 min) 70% TOC decay (60 min)	[21]
Diclofenac (29.6 mg/L)	Fe-ZSM5 (2 mM)	UVA lamps (λ = 365 nm)	$[H_2O_2]_0$ = 50 mM, pH= 4	99% removal (120 min) 66% TOC decay (120 min)	[23]
Paracetamol (100 mg/L)	Cu/Fe-PILC (50 mg/L)	8 W Hg lamp (λ = 254 nm)	$[H_2O_2]_0$ = 13.4 mM, pH = 5.5	100% removal (60 min) 80% removal (180 min)	[24]
p-aminobenzenesulfanilamide (56.6 mg/L)	Fe-pillared clay (1 g/L)	15 W UV-C lamps (λ = 254 nm)	$[H2O2]_0$ = 5.2 mM, pH = 5.2	100% removal (60 min) 52% TOC decay (180 min)	[25]
Tetracycline hydrochloride (100 mg/L)	Fe-rectorite (0.4 g/L)	500 W LED lamp (solar simulator)	$[H_2O_2]_0$ = 10 mM, pH= 7	100% removal (150 min)	[27]
Sulfamethoxazole (10 mg/L)	Fe (III)/ alginate (0.5 g/L)	8 W UVA lamp (λ = 365 nm)	$[H_2O_2]_0$ = 0.5 mM, pH= 5.5	90% removal (60 min)	[28]
Tetracycline hydrochloride (20 mg/L)	PVA/SA-$FeCl_3$ (1 g/L)	300 W LED lamp (λ = 420 nm)	$[H_2O_2]_0$ = 6 mM, pH= n.a.	90.5% removal (60 min) 29% TOC decay (60 min)	[29]
Sulfamethoxazole (5 mg/L)	$NiFe_2O_4$- MWCNTs (0.025 g/L)	100 W Hg lamp	$[H_2O_2]_0$ = 40 mM, pH= 5	100% removal (120 min) 68% TOC decay (120 min)	[30]
Norfloxacin (500 mg/L)	Fe_3O_4-MWCNTs (1.2 g/L)	300 W Xe lamp (λ > 420 nm)	$[H_2O_2]_0$ = 98 mM, pH= 3	90% removal (180 min) 85% TOC decay (180 min)	[31]
Tetracycline hydrochloride (43.7 mg/L)	Fe_3O_4 @AC (0.11 g/L)	4 W UC-C lamp	$[H_2O_2]_0$ = 1.97 mM, pH= 3	79% removal (44 min) 44% TOC decay (120 min)	[33]
Metronidazole (20 mg/L)	C_3N_4 @$MnFe_2O_4$-GO (1 g/L)	300 W Xe lamp (λ = 400 nm)	$[PS]$ = 0.01 mM, pH n. a.	94.5% removal (60 min) 83% TOC decay (90 min)	[34]
Amoxicillin (20 mg/L)	C_3N_4 @$MnFe_2O_4$-GO (1 g/L)	300 W Xe lamp (λ = 400 nm)	$[PS]$ = 0.01 mM, pH n. a.	84.3% removal (60 min) 75% TOC decay (90 min)	[34]
Tetracycline hydrochloride (20 mg/L)	C_3N_4 @$MnFe_2O_4$-GO (1 g/L)	300 W Xe lamp (λ = 400 nm)	$[PS]$ = 0.01 mM, pH n. a.	91.5% removal (60 min) 90% TOC decay (90 min)	[34]
Ciprofloxacin (10 mg/L)	C_3N_4 @$MnFe_2O_4$-GO (1 g/L)	300 W Xe lamp (λ = 400 nm)	$[PS]$ = 0.01 mM, pH n. a.	64.6% removal (60 min) 56% TOC decay (90 min)	[34]
Tetracycline hydrochloride (40 mg/L)	α-Fe_2O_3 @g-C_3N_4 (0.5 g/L)	100 W LED lamp (λ = 420 nm)	$[H_2O_2]_0$ = 10 mM, pH= 3.23	92% removal (60 min)	[35]
Tetracycline hydrochloride (50 mg/L)	g-C_3N_4/FeOCl (0.1 g/L)	300 W Xe lamp (λ > 420 nm)	$[H_2O_2]_0$ = 80 mM, pH= 3	90% removal (20 min)	[39]
Tetracycline hydrochloride (20 mg/L)	Fe-POM/ g-C_3N_4 (1 g/L)	300 W Xe lamp (λ < 420 nm)	$[H_2O_2]_0$ = 10 mM, pH= 4	96.5% removal (18 min) 78% TOC decay (18 min)	[40]
Tetracycline hydrochloride (20 mg/L)	10% α-Fe_2O_3/BiOI (1 g/L)	Xe lamp (λ < 420 nm)	$[H_2O_2]_0$ = 10 mM, pH= 6.5	82.1% removal (30 min)	[41]
Tetracycline hydrochloride (20 mg/L)	ZIF-8-modified $MnFe_2O_4$ (0.3 g/L)	300 W Xe lamp (λ > 420 nm)	$[H_2O_2]_0$ = 50 mM, pH= 5.23	92% removal (90 min)	[42]
Ofloxacin (30 mg/L)	Biogenic Fe-Mn oxides (5 mg/L)	500 W Hg lamp (λ < 420 nm)	$[H_2O_2]_0$ = 4.1 µM, pH= 6.8	98.1% removal (120 min)	[47]
Ofloxacin (10 mg/L)	FeC_6-sepiolite (0.5 g/L)	300 W Xe lamp (λ > 420 nm)	$[H_2O_2]_0$ = 2 mM, pH= 3	92.89% removal (150 min) 89% TOC decay (150 min)	[48]
Ornidazole (20 mg/L)	Natural soil (0.033 g/L)	Sunlight (941 W/m^2)	$[H_2O_2]_0$ = 1 mM, pH= 3	95% removal (180 min) 47% TOC decay (180 min)	[50]
Ofloxacin (20 mg/L)	Natural soil (0.020 g/L)	Sunlight (941 W/m^2)	$[H_2O_2]_0$ = 2 mM, pH= 3	92% removal (180 min) 50% TOC decay (180 min)	[50]
Ciprofloxacin (3.31 mg/L)	α-Fe_2O_3 (0.16 g/L)	11 W UV lamp (λ = 3 95 nm)	$[H_2O_2]_0$ = 24 mM, pH= 7.4	58.82% removal (60 min)	[51]
Ciprofloxacin/Fluoxetine (100 µg/L each)	Fe-citrate (1 µM)	15 W UV-A lamp (λ = 365–410 nm)	$[H_2O_2]_0$ = 50 µM, pH = 4.5	80% removal (20 min) 50% TOC decay (90 min)	[52]
Sulfamethoxazole (5 mg/L)	Ferrocene (0.25 g/L)	1000 W Xe lamp (solar simulator)	$[H_2O_2]_0$ = 25 mM, pH= 3	100% removal (120 min)	[60]
Sodium sulfadiazine (5 mg/L)	MIL-100(Fe) (1 g/L)	300 W Xe lamp (λ > 420 nm)	$[H_2O_2]_0$ = 98 mM, pH= 4	79% removal (90 min)	[62]
Sulfamethazine (50 mg/L)	CuFeO (0.5 g/L)	300 W Xe lamp (λ > 420 nm)	$[H_2O_2]_0$ = 60 mM, pH= 6	95.4% removal (30 min) 50% TOC decay (30 min)	[63]
Amoxicillin (50 mg/L)	Fly ash (1 g/L)	UV lamp	$[H_2O_2]_0$ = 10 mM, pH= 7	36.1% removal (240 min)	[67]
Tetracycline hydrochloride (20 mg/L)	$Bi_{3.64}Mo_{0.36}O_{6.55}$/ $CuBi_2O_4$ (1 g/L)	300 W Xe lamp (λ > 420 nm)	$[H_2O_2]_0$ = 60 mM, pH= 7	82.7% removal (30 min)	[70]
Diclofenac (40 mg/L)				95% removal (60 min)	[76]

Table 1 (*continued*)

Pharmaceutical (concentration)	Catalyst (concentration)	Light source	Operational conditions	Removal and TOC decay	Ref.
	3% Cu doped-α-FeOOH (0.4 g/L)	500 W LED lamp ($\lambda = 420$ nm)	$[H_2O_2]_0 = 100$ mM, pH= 6.12		
Diclofenac (30 mg/L)	MS [60.90% Fe_2O_3] (26.6 mg/L)	Simulated sunlight ($\lambda = 300$–500 nm)	$[H_2O_2]_0 = 5$ mM, pH= 7	100% removal (90 min) 87% TOC decay (300 min)	[77]
Acetaminophen (5 mg/L)	Fe_2O_3-TiO_2-bentonite (0.25 g/L)	Xe lamp (solar simulator)	$[H_2O_2]_0 = 0.65$ mM, pH= 3.5	100% removal (60 min) 39% TOC decay (240 min)	[78]
Antipyrine (5 mg/L)	Fe_2O_3-TiO_2-bentonite (0.25 g/L)	Xe lamp (solar simulator)	$[H_2O_2]_0 = 0.80$ mM, pH= 3.5	100% removal (240 min) 24% TOC decay (240 min)	[78]
Ciprofloxacin/ Sulfamethoxazole/ Trimethoprim (10 mg/L each)	Fe_2O_3-TiO_2 film (0.32 mg/cm²)	1500 W solar simulator	$[H_2O_2]_0 = 2.5$ mM, pH= 2.8	66% removal (240 min)	[135]
Amoxicillin (20 mg/L)	TiO_2/GO/Fe_2O_3 (0.5 g/L)	Low pressure Hg lamps	$[H_2O_2]_0 = 20$ mM, pH= 3	88.5% TOC decay (120 min)	[136]
Tetracycline hydrochloride (40 mg/L)	Fe_2O_3 @void@TiO_2 (0.25 g/L)	300 W Xe lamp ($\lambda = 420$ nm)	$[H_2O_2]_0 = 0.377$ M, pH= 9	ca. 75% removal (6 min)	[137]
Pentoxifylline (50 mg/L)	Fe-TiO_2 (0.65 mg/cm²)	UV lamp	$[H_2O_2]_0 = 26$ mM, pH= 4, Q = 0.8 L/min	91% TOC decay (240 min)	[138]
Tetracycline hydrochloride (96 mg/L)	Fe7Ni3S (0.1 g/L)	Visible-light lamp	$[H_2O_2]_0 = 5$ mM, pH= 7	90.5% removal (20 min)	[139]
5-fluorouracil (1 mg/L) cyclophosphamide (2 mg/L)	$Fe_{2.75}Cu_{0.25}O_4$ (0.125 g/L)	UV lamp ($\lambda = 320$–400 nm)	$[H_2O_2]_0 = 15$ mM, pH= 6.5	> 97% removal (150 min)	[140]
Cephalexin (10 mg/L)	Zn-doped Fe_2O_3 HSMS (1 g/L)	300 W Xe lamp ($\lambda > 420$ nm)	$[H_2O_2]_0 = 12$ mM, pH= 4	90% removal (180 min) 60% TOC decay (180 min)	[141]
Paracetamol (100 mg/L)	Fe-ZSM-5 (2 g/L)	450 W Hg lamp ($\lambda = 280$–310 nm)	$[H_2O_2]_0 = 28$ mM, pH= 2.8	100% removal (300 min) 60% TOC decay (300 min)	[142]
Metronidazole (6 mg/L)	Fe/Si/TiO_2 (1 g/L)	220 W Xe lamp ($\lambda = 400$ nm)	$[H_2O_2]_0 = 10$ mM, pH= 7	93% removal (50 min)	[143]
Tetracycline hydrochloride (20 mg/L)	$(Mg,Ni)(Fe,Al)_2O_4$ (0.75 g/L)	Xe lamp	$[H_2C_2O_4]_0 = 1$ mM, pH= 3	91,9% removal (180 min)	[144]
Tetracycline hydrochloride (40 mg/L)	0.1% CuS/Bi_2WO_6 (1 g/L)	300 W halide lamp ($\lambda = 420$ nm)	$[H_2O_2]_0 = 60$ mM, pH= 7	73% removal (50 min)	[145]
Tetracycline hydrochloride (50 mg/L)	TiO_2/Fe_3O_4 (0.3 g/L)	10 W UV-C lamp ($\lambda = 420$ nm)	$[H_2O_2]_0 = 10$ mM, pH= 7	98% removal (60 min) 64% TOC decay (120 min)	[146]
Tetracycline hydrochloride (300 mg/L)	MIL-53(Fe) (0.2 g/L)	300 W Xe lamp ($\lambda = 420$–780 nm)	[PS] = 8.0 mM, pH = 3.45	99.7% removal (80 min)	[147]
Tetracycline hydrochloride (20 mg/L)	$FeNi_3$/SiO_2/CuS (0.005 g/L)	500 W Xe lamp ($\lambda = 420$ nm)	$[H_2O_2]_0 = 4.16$ mM, pH = 9	83% removal (200 min)	[148]

AC: activated carbon, GO: graphene oxide, MS: metallurgical slag, ZSM5: Zeolite Sonony Mobil-5, ZIF-8: Zeolitic imidazolate framework, FH: Ferrihydrites, MWCNTs: magnetic walled carbon nanotubes, HSMS: hollow sphere mesocrystals, MIL: Material Institute Lavoisier, PVA/SA: poly (vinyl alcohol)/sodium alginate, POM: polyoxometalates, PILC: pillared clay.

$$e^- \text{ (conduction band)} + O_2 \rightarrow O_2^{\bullet -} \tag{6}$$

$$h^+ \text{ (valence band)} + H_2O \rightarrow H^+ + {}^{\bullet}OH \tag{7}$$

$$h^+ \text{ (valence band)} + OH^- \rightarrow {}^{\bullet}OH \tag{8}$$

$$H_2O_2 + e^- \rightarrow {}^{\bullet}OH + OH^- \tag{9}$$

$$Fe^{3+} + e^- \rightarrow Fe^{2+} \tag{10}$$

$$Fe^{3+} + h\nu + OH^- \rightarrow Fe^{2+} + {}^{\bullet}OH \tag{11}$$

Many authors have reported the use of iron oxides/H_2O_2 systems for the removal of drugs in aqueous solution at pH values ranging from 3 to circumneutral [13]. Mameri et al. [15] studied the degradation of paracetamol with goethite (α-FeOOH)/ H_2O_2/UV and achieved only 45% degradation after 180 min of treatment. The slow degradation rates, regardless of pH, are due to the adsorption of paracetamol on the goethite surface, not generating enough ROS to mineralise the contaminant. This effect is generally attributed to the blocking of the catalytic sites, which prevents the α-FeOOH action from regenerating Fe (II) and additional ROS as a photoredox activator (Eq. (12)).

$$\equiv Fe\,(OH^-) + h\nu \rightarrow \equiv Fe\,(OH^-)^{\bullet} \rightarrow \equiv Fe + {}^{\bullet}OH \tag{12}$$
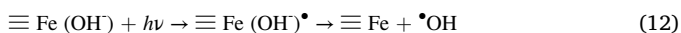
Although a number of iron oxide compounds have been used as heterogeneous photo-Fenton catalysts, ferrites (with the general molecular formula $M_xFe_{3-x}O_4$, where M is a divalent transition metal ion) have been the focus of research due to their high stability and narrow band gap leading to activity under visible-light. The use of copper ferrite (Cu-Fe_2O_4) was described by Gao et al. [16] for the degradation of sulfamethoxazole at circumneutral pH. Under optimal conditions, almost complete degradation of the parent compound and around 32% mineralisation was achieved after 120 min of treatment. The mechanistic study showed that large concentrations of the reactive oxygen species were formed on the Cu-Fe_2O_4 surface, which was attributed to the ordered pore structures and the large surface area of the mesoporous catalyst.

Hermosilla et al. [17] reported the development of an eco-friendly manganese ferrite (Mn-Fe_2O_4) catalyst and tested this material for the degradation of two biorecalcitrant compounds, ciprofloxacin and carbamazepine. The key to this study was a mechanism by which the catalyst could be easily removed from the treated water to allow reuse. Therefore, the inherent magnetic property of the α-Fe_2O_3 (weakly ferromagnetic material at room temperature) was exploited. While the material removed 95% of the original ciprofloxacin, only 25% of the carbamazepine was removed. Lai et al. [18] investigated manganese-ferrite as a photocatalyst for the degradation of tetracycline and achieved more than 90% removal after 120 min at natural pH (pH 5.5).

Strategies to increase the specific surface area of the catalyst and improve photon absorption traditionally exploit the morphology and microstructure of photocatalysts, so research activities have increased to develop novel morphologies, including yolk-shell approaches. Xiang et al. [19] synthesised magnetic $ZnFe_2O_4$ microspheres in yolk-shell form by a self-guided solvothermal method and tested the materials for the degradation of tetracycline. They reported that their structure leads to an increased number of active sites, with an additional catalytic effect resulting from multiple scattering/refraction of photons within the inner-yolk structure.

Considerable efforts have been made to develop iron-based minerals such as haematite, goethite, and wüstite for the photo-Fenton process, allowing the potential use of oxygen as an electron acceptor, which from a practical standpoint could eliminate the need for a continuous supply of H_2O_2; however, there are no reports of applications for the removal of pharmaceutical compounds.

Research comparing the application of α-FeOOH, Fe_3O_4 (magnetite) and γ-Fe_2O_3 (maghemite) reported low catalytic activity at the standard neutral pH of wastewater, but the materials showed potential for rapid removal and multiple reuse [13]. In an attempt to increase efficiency and utilise magnetic separation, a combination of α-FeOOH and γ-Fe_2O_3 was considered for tetracycline removal [20]. Mechanism studies suggest γ-Fe_2O_3 pairs can trap photogenerated electrons in the conduction band of α-FeOOH inhibiting the reaction between electrons and H_2O_2, so that the separated holes can accelerate the production of singlet oxygen from H_2O_2 (Eq. (13)).

$$h^+ \text{ (valence band)} + H_2O_2 \rightarrow O_2^{\bullet-} + 2H^+ \qquad (13)$$
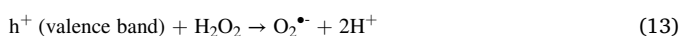
Natural iron oxide composites, such as ferrihydrite, have been considered as alternative photo-Fenton catalysts. As it is well known, surface-mediated iron regeneration leads to an improvement in photo-catalytic activity and a reduction in H_2O_2 consumption [21]. Huang et al. [21] studied the degradation of tetracycline with 15% $yCeO_2$/ferrihydrite reporting complete degradation after 60 min of treatment. Analysis of the underlying mechanism showed that the incorporation of $yCeO_2$ accelerated the Fe^{2+} regeneration cycle, leading to the production of photogenerated electrons. These results are supported by Jiang et al. [22], who reported the use of 7% TiO_2/Fh as an efficient photocatalyst for cefotaxime degradation.

Although many reports have described the development of heterogeneous perovskite-based photocatalysts for the removal of organic compounds by photo-Fenton processes [13], to the author's knowledge, there are no publications investigating the removal of pharmaceutical compounds. Since the step of regeneration of ferrous ions (Eq. (10)) is the main limiting factor in Fenton-based processes, many researchers have proposed the use of electron-rich materials in combination with the Fenton catalyst to accelerate the regeneration of ferrous ions. Support materials such as zeolites [23], clays [24,25] and silica have been used to prevent the leaching of metallic iron while providing large surface area, good thermal stability, high mechanical strength, resistance to organic solvents and additional electrons for the reaction systems [26].

Pillared clays have been reported to be applicable by the addition of oxygenated-metal cations, resulting in increased photocatalytic activity due to an increase in porosity and surface area. Such effects were reported by Hurtado et al. [24], who assessed the use of Cu/Fe pillared clay as a catalyst for the mineralisation of paracetamol by photo-Fenton processes under circumneutral pH conditions. They reported around 80% mineralisation, only 2% less than under acidic conditions – which is due to the fact that the presence of Cu promotes the formation of additional reactive oxygen species. The activity and stability of these catalysts depend on the molar ratio of the metals, with the Cu content being about 15 times lower than the Fe content. Similarly, the use of rectorite as a support was proposed by Guo et al. [27], who investigated the removal of tetracycline. They reported around 95% pollutant removal in a pH range of 3.8–8.1 under natural sunlight. The mesoporous structure of these materials favours molecular diffusion of H_2O_2 and pollutants and, in conjunction, with the presence of goethite, likely enhances electron transfer and thus, the overall rate of pollutant degradation.

Polymer matrix composites have also attracted attention due to their high adsorption capacity for pollutants and ease of fabrication, leading to systems that prevent catalyst agglomeration and allow catalyst reuse. The high catalytic activity of iron alginate beads resulted in significant degradation of drugs in batch and continuous operation, with negligible iron leaching [28]. Nevertheless, there are several problems associated with the use of alginate, including matrix degradation, mass transfer limitations, large pore size, and perhaps most importantly, low mechanical strength of the composite. The addition of cross-linking polymers such as chitosan or polyvinyl alcohol has been reported to improve the physical and mechanical properties without loss of catalytic efficiency [29].

Carbon-based materials such as carbon nanotubes [30,31], activated carbon [32,33], graphene oxide [34], biochar [18] and g-C_3N_4 [35] have been successfully used as photocatalyst supports for the removal of pharmaceutical compounds. Graphene oxide (GO) has been reported to act as a sacrificial electron donor on Fe_3O_4 catalysts (Fe_3O_4 @GO), as the unpaired π electrons of sp^2 hybridised carbon atoms are transferred to Fe_3O_4 and accelerate both the Fe^{2+} regeneration step and the overall catalytic efficiency. The application of g-C_3N_4 @$MnFe_2O_4$ @GO was reported by Wang et al. [34] for the degradation of metronidazole, amoxicillin, tetracycline, and ciprofloxacin using persulfate (Fenton-like process) as oxidant under visible light irradiation [36]. These ternary composites increased catalytic activity, resulting in 94.5% removal of metronidazole, about 3.5 times that of bare g-C_3N_4. The authors attributed the additional removal to the increased adsorption of organic compounds due to 1) the presence of functional states on the GO surface e.g. carboxyl and hydroxyl groups and 2) hydrophobic interactions, hydrogen bonding, π—π interactions and electrostatic interactions [37].

The large surface area of g-C_3N_4 nanosheets as supports for iron catalysts provides additional entrapment of iron species due to the high-density of N atoms and "six-fold cavities" [38]. Recent studies with these materials have showed the inclusion of α-Fe_2O_3 is effective against tetracycline in a broad pH range from 2.11 to 9.09 [35]. They have described a solid-state Z-scheme carrier transfer mechanism with photoluminescence analysis indicating increased separation efficiency of photogenerated electron/hole pairs by hybridisation. The generation of additional electrons in turn contributes to the regeneration step of Fe^{2+}increasing the production of hydroxyl radicals, and ultimately enhancing the rate of antibiotic degradation. Similar results were obtained by Zhao et al. [39] who synthesised a g-C_3N_4/FeOCl composite with Z-scheme for the total degradation of tetracycline.

Research has shown the introduction of nitrogen holes into the electronic structure can generate multiple unpaired electrons, which improves both charge separation and transfer efficiency. In addition, the incorporation of N can change the energy band structure, increasing the absorption of visible light, as confirmed by the analysis of electron paramagnetic resonance studies [40]; nevertheless, further studies are required to verify the effects of visible light.

Many studies have indicated the incorporation of semiconductors (metal oxides, metal sulphides, metal vanadates/molybdates/phosphates, and metal-free graphitic carbon nitride, g-C_3N_4) with increased carrier density, likely contributes to an increase in photo-Fenton process effectiveness [41,42]. The inclusion of iron species in the composite catalyst can promote the use of visible light by acting as photosensitisers and charge injectors. Depending on the oxidation state of the iron species, the resulting Fe/TiO_2 composites can be classified as lattice-doped, surface-modified, or heterojunction structures. In lattice doping, iron ions replace Ti^{4+} substituents in the crystalline TiO_2 structure, and in surface modification, iron oxide nanoparticles or amorphous iron species are usually immobilised as goethite on the TiO_2 surface, with heterojunction structures resulting from higher iron loading in the composite.

2.2. Application of photo-Fenton catalysts for the removal of pharmaceuticals

Our dependence on pharmaceuticals, including antibiotics, results in widespread occurrence of both their parent compounds and metabolites in the aquatic environment [43,44] and new technologies are required to remove such compounds from wastewater streams due to their chronic and acute effects.

2.2.1. Antibiotics

Fluoroquinolones, derived from nalidixic acid, share a common ring structure based on the presence of a carboxyl group and a ketone and exhibit remarkable antibacterial properties. The presence of fluorine distinguishes fluoroquinolones from quinolones and enhances their activity against gram-positive and negative bacteria. These important structural features provide inherent chemical and biological stability. After use in humans and animals, a large proportion of fluoroquinolones are excreted into the environment via urine and faeces, both the parent molecule and metabolites. This class of drugs has been detected in wastewater, groundwater, surface water, soils and sediments, reflecting low removal efficiency. For example, ofloxacin, a common fluoroquinolone, has been quantified in effluents from WWTPs in Beijing, Hangzhou, and Vancouver at concentrations ranging from 0.6 to 1405 ng/L [1,45,46]. Many studies have demonstrated the application of the photo-Fenton process for the removal of recalcitrant compounds such as fluoroquinolones. In particular, Du et al. [47] assessed the removal of ofloxacin using biogenic Fe-Mn oxides produced by *Pseudomonas sp*. Analytical methods showed the synthesised catalyst had an amorphous layered structure, a broad absorption spectrum, and a low charge resistance. According to the experimental results, both photogenerated electron/hole pairs and hydroxyl radicals contributed to the degradation of ofloxacin, while the superoxide anion radical made a negligible contribution. To determine whether the reaction intermediates formed by photo-Fenton were more toxic than the parent compound, microbial respiratory inhibition analysis was performed to evaluate toxicity. The results were promising, as the toxicity was significantly reduced (47%), although further studies were suggested to evaluate the catalytic stability. Tian et al. [48] also investigated the removal of ofloxacin; however, their approach used highly dispersed iron-carbide cluster anions (FeC6) on sepiolite as a photocatalyst. In the experiments, 92.89% was achieved after 150 min of treatment with a 300 W Xe lamp. As shown in Table 1, this synthesised photocatalyst showed higher activity in the mineralisation of ofloxacin (89.35%) compared to previous studies [49,50]. Transmission electron microscopy (TEM) and density functional theory attributed the catalytic activity of Tian's materials to the incorporation of ferrocene into sepiolite via a Si—O—C—Fe bond, resulting in a high dispersion of electrodeficient ferrocene. This played a role in promoting the iron regeneration cycle by forming an Fe-H$_2$O$_2$ complex at the surface. High mineralisation rates, 98.7% F atoms and 97% N atoms were converted to inorganic ions, indicating high removal of associated toxicity. However, the need for complementary technologies such as ion exchange and/or biological denitrification, was highlighted to ensure adequate water quality after oxidation treatment.

The degradation of ciprofloxacin was performed by Hakimi and Alikhani [51], who analysed the removal of ciprofloxacin from aqueous solution using hexagonal α-Fe$_2$O$_3$ nanoparticles. They attained a 59% reduction of the parent compound with a low catalyst dosage at pH 7.4, probably due to the presence of the zwitterionic form of the drug. Similarly, Perini et al. [52] studied the photo-Fenton degradation of ciprofloxacin at ppb concentrations in anaerobically pretreated hospital wastewater. Negligible degradation and mineralisation were observed after 90 min, which was attributed to the high content of recalcitrant compounds formed during the anaerobic degradation process, namely low molecular weight carboxylates and alcohols well-known to inhibit Fenton reactions. In addition, the interception reactions (Eqs. (14) and (15)) were attributed to the presence of inorganic carbon in the form of bicarbonate and carbonate in the main solution.

$$\bullet OH + HCO_3^- \rightarrow H_2O + CO_3^- \tag{14}$$

$$\bullet OH + CO_3^{2-} \rightarrow HO^- + CO_3^{\bullet-} \tag{15}$$

Photo-Fenton based degradation of norfloxacin was investigated by Shi et al. [31] using ferric oxide nanoparticles on multi-walled carbon nanotubes. X-ray diffraction (XRD) analysis confirmed that the nanoparticles had a low crystalline Fe$_3$O$_4$ concentration, with the iron oxide in the form of inverse spinel structure. Significant adsorption of norfloxacin was observed, promoting photodegradation on the surface of the photocatalyst with minimal iron leaching. The material was successfully recycled and performed well after five consecutive runs, demonstrating the stability of the nanoparticles after successive oxidation cycles.

Sulphonamides are synthetic antimicrobial agents containing the sulphonamide group and the amino group at the para-position of the benzene ring. They were developed to affect folate synthesis in microbes and eventually purine and DNA synthesis. The introduction of multiple substituents results in structural products with altered physicochemical, pharmacokinetic, and pharmacodynamic properties [53]. Most sulphonamides are polar compounds and water-soluble, thus, they have been detected in many environmental matrices such as water, soil, and sediment [54,55]. In particular, sulfamethoxazole is detected in wastewater, surface water, and drinking water at concentrations of 100–2500, 60–150 and 12 ng/L, respectively [56–58]. Due to the inefficiency of conventional wastewater treatments in removing low concentrations of antibiotics, many authors have tested photo-Fenton as an alternative for the removal of sulfamethoxazole [16,28,30,56]. For example, Nawaz et al. [30] evaluated their degradation with a MWCNTs-NiFe$_2$O$_4$ composite prepared by a one-step hydrothermal treatment. They reported that the magnetically recyclable catalyst possessed high photocatalytic activity due to the synergistic effect between NiFe$_2$O$_4$ and MWCNTs. The effective charge separation inhibited the recombination of electron/hole pairs, and thus, increased the generation rates of reactive oxygen-containing species, mainly hydroxyl radicals. Moreover, the presence of the iron-hydroxy complex was able to absorb ultraviolet and visible energy and promote the generation of hydroxyl radicals (Eq. (16)) [10,59].

$$Fe\,(OH)^{2+} + h\nu \rightarrow Fe^{2+} + \bullet OH \tag{16}$$

Similar results were obtained by Gao et al. [16], who reported the synthesis of 3D-ordered mesoporous CuFe$_2$O$_4$ (inverse spinel structure) as heterogeneous photo-Fenton catalysts for the removal of sulfamethoxazole at circumneutral pH. The use of Fe (III)/ alginate beads was proposed by Cruz et al. [28], who reported 90% removal of sulfamethoxazole at pH 5.5 after 60 min of treatment. However, the pH of the solution and the attack of hydroxyl radicals on the alginate resulted in instability of the catalyst. Under highly acidic conditions (pH ~ 2–3), remarkable iron leaching was observed, accompanied by an increase in TOC, indicating a breakup of the polymer matrix, effectively leading to a homogeneous process. Li et al. [60] evaluated the use of ferrocene as a photocatalyst for the degradation of sulfamethoxazole under simulated sunlight attaining complete removal after 120 min of treatment. From their results, they concluded that the family of sulphonamides based on a six-membered heterocyclic ring exhibited similar sensitivity and reactivity to hydroxyl radicals, whereas different degradation behaviour was observed for five-membered heterocyclic ring structures. These results are in agreement with those of Ji et al. [61], who had previously assessed the degradation of several sulphonamides by thermoactivated persulfate oxidation. The influence of dissolved organic matter, inorganic carbon and halide ions on the degree of degradation was found to be negligible. Despite the positive results of this study, the evaluation of toxicity and antimicrobial activity resulting from the production of degradation products should be confirmed.

The degradation of another example from the sulphonamide group, sulfadiazine, was described by Tian et al. [62]. For this purpose, they synthesised a magnetic catalyst based on MIL-100 (Fe) with Fe$_3$O$_4$, which was prepared as novel nanorods via a sustainable one-pot synthesis process. The magnetisation curve exhibited typical superparamagnetic properties, that allowed magnetic separation with a conventional magnet at 23 emu/g. After five consecutive runs with the catalyst under optimal experimental conditions, 79% degradation was

attained, demonstrating plausible photocatalytic stability/reusability. Cheng et al. [63] also investigated the degradation of sulfadiazine at circumneutral pH using a magnetic Cu-Fe oxide – again focusing on the recyclable aspects of photo-Fenton catalysis. The catalyst showed remarkable photocatalytic activity over a broad pH range, with more than 95% of the parent compound removed after 30 min of treatment at near neutral pH (pH = 6.0). The H_2O_2 activation mechanism was investigated by radical scavenging and electron-spin trapping experiments, suggesting a synergistic effect between photoinduced electrons and the presence of the transition metals in the metal oxide.

Penicillin-based compounds belonging to the β-lactam family of antibiotics, have been widely used as antibiotics in human and veterinary therapy since their discovery in 1928. The subgroup of aminopenicillins, which includes amoxicillin, ampicillin, epicillin, and bacampicillin, have an additional amine group on their side chain [64] and are commonly prescribed. Although amoxicillin is rapidly hydrolysed under mild acidic and basic conditions, its degradation by photo-Fenton has been extensively investigated mainly because of the formation of numerous degradation products, that may be more resistant and indeed more toxic than the parent compound [65,66]. Ramírez-Franco et al. [67] analysed amoxicillin degradation using a magnetic TiO_2 @GO@Fe_3O_4 composite in a photocatalytic reactor with a submerged magnetic membrane. The GO nanosheets were assembled via non-covalent interactions such as electrostatic and π-π stacking on the surface of the TiO_2 particles, which was confirmed by TEM images. The presence of numerous oxygen-containing groups on the GO surface served as anchoring sites for Fe_2O_3 nanoparticles. In degradation experiments, degradation of more than 90% of amoxicillin was achieved after 120 min under optimal conditions. Increasing the Fe_3O_4 concentration on the catalyst promoted agglomeration, resulting in decreased surface area and inhibition of light absorption, which reduced the amoxicillin removal efficiency. As for the degradation mechanism, the electrophilic attack on the nitrogen atom mediated by hydroxyl radicals cleaved the ring structure and promoted further oxidation. Similarly, Wang et al. [34] reported the application of the p-n heterojunction g-C_3N_4 @$MnFe_2O_4$ @GO as a heterogeneous catalyst for the degradation of amoxicillin. Ramírez-Franco et al. [67] investigated a heterogeneous photo-Fenton catalyst based on fly ash (consisting a mixture of metal oxides including SiO_2 (51.5%), Fe_2O_3 (9.37%) and TiO_2 (1.08%) and reported a high degree of pollutant removal.

Tetracyclines are widely used worldwide for antimicrobial treatment. Their amphoteric nature and high stability at acidic and neutral pH allow passage through the gut and thus transfer to many aquatic environments [68], where they have been detected in surface water (up to 8.1 ng/L), municipal wastewater (over 1000 ng/L) and soil (between 86.2 and 198.7 μg/kg) [69]. Compared to other technologies, photo-Fenton has attracted great interest for the removal of tetracycline at relatively low concentrations [19,34,40,41]. Guo et al. [70] assessed the efficacy of 3D-rod-shaped $Bi_{3.64}Mo_{0.36}O_{6.55}$/$CuBi_2O_4$ materials as heterogeneous photocatalysts, attaining 82.7% tetracycline removal after 30 min. Studies showed the nanocomposites exhibited high photocurrent response and the photogenerated charge recombination was limited in the heterostructured materials. A high level of tetracycline degradation (98.7% in 60 min) was also reported using a novel bio-templated ceria-modified ferrihydrite [21]. These results confirm the importance of appropriate addition of Ce to ensure enhanced photodegradation, resulting from Ce^{4+}/Ce^{3+} flux and the generation of photogenerated electrons on the semiconductor surface.

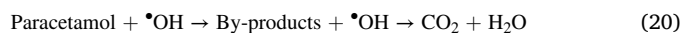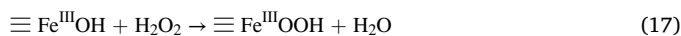### 2.2.2. Non-steroidal anti-inflammatory drugs (NSAIDs)

Acidic pharmaceuticals, primarily non-steroidal anti-inflammatory drugs (NSAIDs) are the most commonly detected over-the-counter drugs in aquatic ecosystems due to their widespread use as anti-inflammatory, analgesic, or antipyretic therapeutic agents. Their high water solubility and polar nature may compromise the efficacy of their removal by conventional treatments [71–73]. According to the Global Water Research Coalition criteria, NSAIDs such as diclofenac are among the top 10 persistent pollutants. Diclofenac has been detected in surface waters and effluents from municipal WWTPs at μg/L concentrations, causing adverse effects on human health and aquatic organisms [74,75]. Therefore, those working on the development of alternative treatment strategies have paid special attention to this particular pollutant. Xu et al. [76] proposed Cu-doped α-FeOOH nanoflowers as a heterogeneous photocatalyst for the degradation of diclofenac. Scanning electron micrographs (SEM) confirmed the hierarchical, self-assembling 3D structure, with a slight change in surface energy due to Cu doping of the α-FeOOH lattice. The nanostructured catalyst possessed enhanced photocatalytic activity compared to pure α-FeOOH due to lower recombination of photogenerated electrons and holes and rapid electron transfer caused by the presence of copper. An iron-exchanged zeolite (FeZSM5) was evaluated by Perisic et al. [23], where the photocatalyst attained 66% TOC reduction after 120 min of treatment. The initial pH of the solution significantly affected the mineralisation rate, while adjusting the H_2O_2 concentration and Fe content on the zeolite had a negligible effect. They confirmed a synergistic effect of adsorption and oxidation in the overall mechanism of action. In the context of environmental remediation, Arzate-Salgado et al. [77] studied the application of copper slag as a heterogeneous photo-Fenton catalyst for the removal of diclofenac attaining 57% TOC removal after 90 min of treatment. However, the resulting effluent was almost three times more toxic than original diclofenac solution due to partial mineralisation and production of carbazole molecules and myeloperoxidase, which can catalyse peroxide to form less reactive oxygen species [74].

The degradation of antipyrine, another compound of the NSAID family, was studied by Molina et al. [78]. Using a Fe_2O_3-TiO_2-organo/bentonite heterostructure, almost total degradation was observed after 240 min of treatment. The bentonite clay was modified by the interaction of alkylammonium cations to provide a hydrophobic surface that supports the incorporation of TiO_2 with improved crystallinity. The mesoporous catalyst exhibits a disordered layered structure with high dispersed metal oxides. They concluded that antipyrine is similarly robust to azo dyes and acetaminophen due to the pyrazolone ring structure.

Indeed, many researchers have studied the degradation of acetaminophen (also known as paracetamol), which consists of an aromatic benzene ring substituted by an amide group and a hydroxyl group in the p-position. This common non-inflammatory analgesic has been detected in wastewater from European WWTPs at concentrations around 6 mg/L [79] and in the river Tyne at concentrations greater than 65 mg/L [80].

Mameri et al. [15] investigated the use of a goethite system for the removal of paracetamol from aqueous wastewater by photo Fenton process, achieving 45% removal after 180 min of treatment. No iron leaching was observed in the main solution, indicating surface-mediated paracetamol degradation by hydroxyl radicals (Eqs. (17)–(20)).

$$\equiv Fe^{III}OH + H_2O_2 \rightarrow \ \equiv Fe^{III}OOH + H_2O \tag{17}$$

$$\equiv Fe^{III}OOH + h\nu \rightarrow \ \equiv Fe^{IV}\text{-} O + {}^{\bullet}OH \tag{18}$$

$$\equiv Fe^{IV}\text{-} O + H_2O \rightarrow \ \equiv Fe^{III}OH + {}^{\bullet}OH \tag{19}$$

$$Paracetamol + {}^{\bullet}OH \rightarrow By\text{-}products + {}^{\bullet}OH \rightarrow CO_2 + H_2O \tag{20}$$

Hurtado et al. [24] developed an iron-containing clay catalyst and incorporated copper by ion-exchange (Cu/Fe-PILC). They achieved 80% paracetamol mineralisation at both acidic and neutral pH. However, the authors reported the incorporation of Cu decreased the surface area and pore volume, which reduce the absorption capacity.

2.2.3. Radiocontrast agents

Radiocontrast agents, such as barium sulphate and iodinated benzene derivatives, are used to enhance the visibility of internal body structures for imaging procedures such as computed tomography,

magnetic resonance imaging, and/or radiography. They are frequently identified in wastewater streams [81], and their high water solubility and poor biodegradability hinder their removal by conventional treatments [82]. Diatrizoic acid, for example, is a commonly used iodine-containing X-ray contrast agent that has been detected in the environment [83] because undergoes biotic and abiotic transformations that result in the formation of stable transformation products with higher toxicity than the parent molecule. The groups of Sanromán and Oturan evaluated the photochemical degradation of diatrizoic acid using iron sepiolite-based alginate beads and iron-activated carbon as heterogeneous photocatalysts [32]. While the alginate beads exhibited low stability in the presence of H_2O_2 under UV light irradiation [28,29], the activated carbon-supported iron promoted the formation of hydroxyl radicals with negligible leaching. They concluded that the synthesised catalysts were activated by H_2O_2 via heterogeneous Fenton and photo-Fenton reactions, and the catalysis was accelerated by the generation of additional electrons by UVC irradiation.

3. Photocatalysis

Scientific studies of photocatalysis began in the mid-1970 s, and ongoing research has shown the process has great potential for environmental remediation. The mechanism of photocatalysis involves the excitation of electrons from the valence band into the conduction band to generate reactive oxygen species (Fig. 2). Relevant publications related to pharmaceutical mineralisation by photocatalysis are summarised in Table 2.

3.1. Materials used as photocatalysts

The basic properties of active photocatalyst materials include a suitable band gap, good photostability, high carrier mobility, correct band edge potentials, large surface area, and efficient photon absorption. Generally, n-type semiconductors (occupied valence band and unoccupied conduction band) are used as photocatalysts for environmental remediation, with materials selected to have a band gap

corresponding to energy in the ultraviolet region. Metal oxides from the II-IV groups, ZnO, WO_3, and TiO_2, have been successfully used for the degradation and mineralisation of organic pollutants. Most research has focused on TiO_2, which has high activity against a variety of organic contaminants and even complete mineralisation due to its low toxicity, low cost, high chemical stability and wide availability [84]. However, further research is being conducted to improve the efficiency of TiO_2 to overcome electron-hole recombination losses and enhance photon absorption in the visible region of the solar spectrum [85].

From a perspective of a practical application, cost-effective photocatalytic technologies require in-depth studies with ongoing work to create recyclable catalysts via immobilised systems, magnetic particles, flocculation routes, etc., with the primary goal of developing versatile, efficient catalysts with the appropriate functionality.

Numerous researchers have focused on the addition of dopants to modify the physical properties and surface activity and improve the photoreaction to visible light [86]. The use of noble metals such as silver, platinum, palladium, and gold as support materials allows for improved photocatalytic performance; however, this does not always generate large amounts of active radicals. Some benefits have been reported from the formation of bimetallic photocatalysts, in which the electron band structure of the primary metal can be influenced by the electronic properties of the incorporated metal particles. The design of ternary nanostructures allows modification of their elemental composition and optical bandgap [87]; nevertheless, in many cases only limited increase in efficiency has been reported.

The use of novel heterojunction semiconductor materials, such as bismuth oxyhalides (BiOX, X = Cl, Br, I), has attracted much attention from academic researchers due to their response to visible-light and their unique tetragonal matlockite layer structure [88]. For example, BiOCl has been reported to exhibit higher photocatalytic activity under UV irradiation, while BiOI showed significant visible light absorption due to its lower energy band gap. BiOBr revealed good oxidation/reduction activity under ultraviolet-visible light irradiation, which may be attributed to the heterojunction band structure. To improve the photocatalytic behaviour of these materials, BiOX-based composites
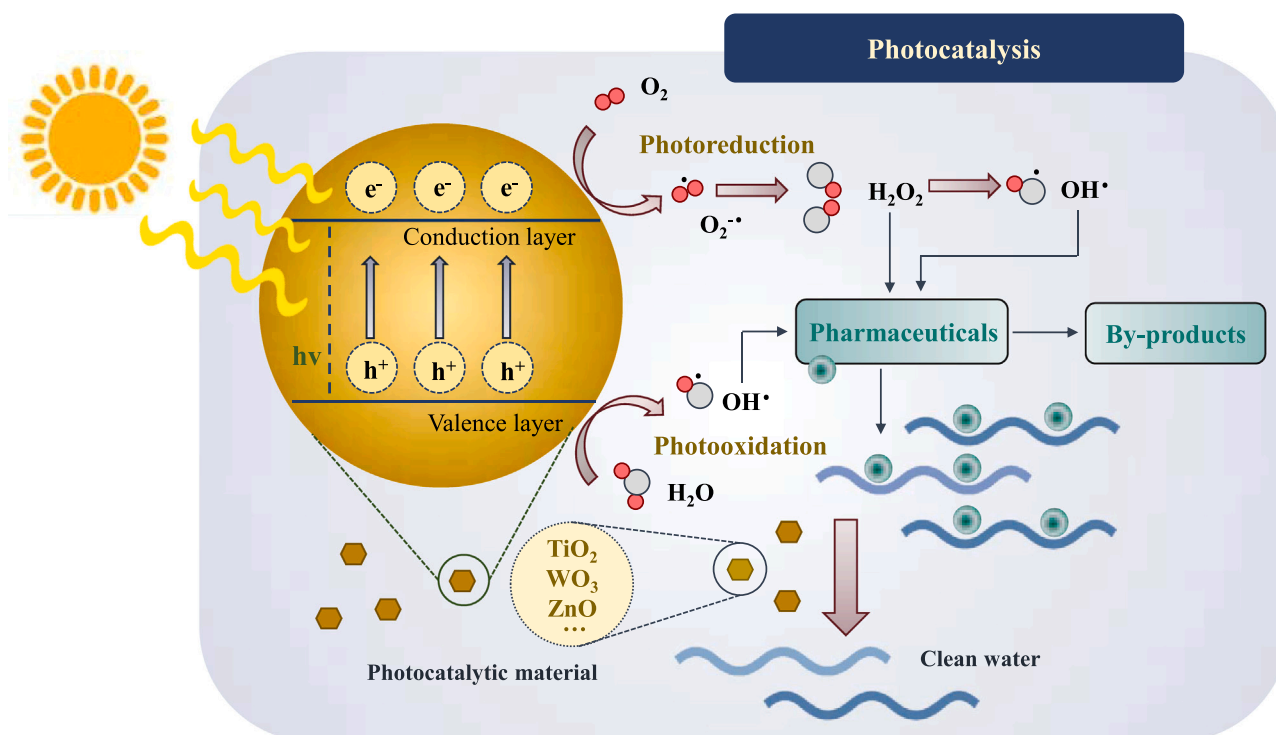

Fig. 2. Photocatalytic mechanism.

Table 2
Summary of some relevant studies on photocatalytic systems.

Pharmaceutical (concentration)	Catalyst (concentration)	Light source	Operational conditions	Removal and TOC decay	Ref.
Azithromycin/Trimethoprim/ Ofloxacin/Sulfamethoxazole (100 µg/L each)	TiO_2 (1 g/L)	9 W LED lamps (λ = 381 nm)	pH n.a.	100% removal (180 min)	[7]
Ciprofloxacin (30 mg/L)	1.5%Ag-TiO_2 (0.5 g/L)	15 W Hg lamp (λ = 254 nm)	pH n.a.	100% removal (30 min) 100% TOC decay (180 min)	[86]
Tetracycline hydrochloride (10 mg/L)	AgBr-TiO_2-Palygorskite (0.5 g/L)	300 W Xe lamp	pH = 9	90% removal (90 min) 67% TOC decay (90 min)	[87]
Tetracycline hydrochloride (20 mg/L)	BiOBr/BiOI/cellulose (0.4 g/L)	500 W Xe lamp ($\lambda \geq$ 420 nm)	pH n.a.	91% removal (60 min)	[88]
Tetracycline hydrochloride (20 mg/L)	CQDs/BiOCl/BiOBr (0.3 g/L)	250 W Xe lamp (λ = 400 nm)	pH n.a.	77% removal (120 min)	[89]
Ibuprofen (80 mg/L)	g-C_3N_4/CQDs/$CdIn_2S_4$ (1 g/L)	300 W Xe lamp (λ = 420 nm)	pH n.a.	91% removal (60 min) 85% TOC decay (60 min)	[90]
Metronidazole (35 mg/L)	Fe^0/GO/TiO_2 (0.2 g/L)	20 W Hg Lamp (λ = 254 nm)	pH = 6.5	99.3% removal (80 min)	[91]
Ciprofloxacin (25 mg/L)	15% BiOBr/TiO_2 (1 g/L)	Visible light	pH = 6	95.5% removal (180 min)	[93]
Ciprofloxacin (10 mg/L)	3% CQDs/BiOBr (0.3 g/L)	300 W Xe lamp ($\lambda \geq$ 400 nm)	pH n.a.	100% removal (240 min) 44.3% TOC decay (240 min)	[94]
Ciprofloxacin (20 mg/L)	WS_2/BiOBr (1 g/L)	500 W Xe lamp ($\lambda \geq$ 420 nm)	pH = 7	83% removal (100 min)	[95]
Sulfamethoxazole (10 mg/L)	TiO_2-biochar (5 g/L)	15 W UV lamp (λ = 254 nm)	pH = 4	75% removal (180 min) 65% COD decay (180 min)	[98]
Sulfamethoxazole (10 mg/L)	ZnO (200 mg/L)	11 W fluorescent (λ = 365 nm)	pH = 7.5	84% removal (60 min)	[99]
Sulfamethoxazole (10 mg/L)	WO_3-CNT (1 g/L)	300 W Xe lamp	pH n.a.	81.9% removal (180 min)	[100]
Sulfamethoxazole /trimethoprim (400 µg/L each)	TiO_2 (0.05 g/L)	LED lamp	pH = 5.6, Q = 8 mL/min	> 90% removal (20 min)	[101]
Tetracycline hydrochloride (30 mg/L)	3% p-C_3N_4/f-BiOBr (1 g/L)	250 W Xe lamp (λ = 400 nm)	pH n.a.	94.3% removal (100 min)	[102]
Tetracycline hydrochloride (10 mg/L)	α-FeOOH/FeS_2 (0.5 g/L)	100 W LED lamp (λ = 400 nm)	pH = 3	95.4% removal (150 min)	[103]
Tetracycline hydrochloride (80 mg/L)	CuO/$BiVO_4$ (0.2 g/L)	300 W Xe lamp	[PMS] = 2 mM, pH = 4.1	100% removal (50 min) 29% TOC decay (50 min)	[105]
Tetracycline hydrochloride (12 mg/L)	20% g-C_3N_4 @Bi/BiOBr (1 g/L)	Solar simulated light (λ > 420 nm)	pH n.a.	78% removal (240 min)	[106]
Ibuprofen (60 mg/L)	TiO_2 (1 g/L)	9 W LED lamps (λ = 381 nm)	pH = 5.3	100% removal (30 min) 53% DOC decay (90 min)	[107]
Diclofenac (10 mg/L)	mont-La (6%)-$Cu_{0.6}Cd_{0.4}S$ (1 g/L)	Hg lamp (λ < 578 nm)	pH = 5.9	92% removal (240 min) 67% TOC decay (240 min)	[108]
Acetaminophen (3 mg/L)	67% $Bi_4O_5I_2$-$TiO2$ (0.5 g/L)	300 W Xe lamp (λ = 400 nm)	pH n.a.	ca. 95% removal (6 min) 83% TOC decay (120 min)	[109]
Acetaminophen (5 mg/L)	In_2S_3/Zn_2GeO_4-30 (1 g/L)	300 W Xe lamp (λ > 420 nm)	pH = 7	93% removal (360 min) 55% TOC decay (360 min)	[110]
Acetaminophen (50 µg/L)	BiOCl (0.3 g/L)	Fluorescent light (λ = 300–500 nm)	pH = 5.4 [$Na_5S_2O_8$] = 1 mM	100% removal (180 min)	[111]
Ketoprofen (15 mg/L)	BiS_3/TiO_2-mont (0.5 g/L)	150 W Hg lamp (λ = 254 nm)	pH = 11	100% removal (120 min) 10% TOC decay (120 min)	[113]
17α-ethinylestradiol (3 mg/L)	WO_3-SBA (1.2 g/L)	20 W Hg lamp (λ = 254 nm)	pH n.a.	98% removal (270 min)	[140]
Isoniazid/Rifampicin (10 mg/L each)	TiO_2 (0.5 g/L)	125 W Hg lamp (λ = 315–400 nm)	pH = 6	90% isoniazid and 60% rifampicin removal (60 min)	[149]
Metronidazole (4 mg/L)	$NiS_{1.0}$–$ZnS_{5.2}$/NC (3 g/L)	35 W Hg lamp (λ = 435.8 nm)	pH = 6	68.97% removal (150 min)	[150]
Metronidazole (2 mg/L)	NiO/SnO_2-NC (1.2 g/L)	35 W Hg lamp (λ = 435.8 nm)	pH = 3	90% removal (180 min) 65% TOC decay (180 min)	[151]
Metronidazole (2 mg/L)	SnS_2-ZnS-NC (3 g/L)	35 W Hg lamp (λ < 435.8 nm)	pH = 3	77.17% removal (250 min)	[152]
Clozapine (5 mg/L)	TiO_2 (300 mg/L)	Xe lamp (solar simulation)	pH = 8.2	100% removal (20 min)	[153]
Alprazolam (9.3 mg/L)	TiO_2 (300 mg/L)	125 W Hg lamp (λ < 366 nm)	pH = 5.6	100% TOC decay (60 min)	[154]
Tetracycline hydrochloride (20 mg/L)	SDS-BiOBr-MB (0.5 g/L)	300 W Xe lamp (λ = 430–600 nm)	pH = 6.3	85% removal (120 min) 39.2% TOC decay (120 min)	[155]
Ciprofloxacin (10 mg/L)	SDS-BiOBr-MB (0.5 g/L)	300 W Xe lamp (λ = 430–600 nm)	pH = 6.3	95% removal (120 min) 39.1% TOC decay (120 min)	[155]
Ciprofloxacin (10 mg/L)	2% g-C_3N_4-$Bi_4O_5Br_2$ (0.5 g/L)	300 W Xe lamp ($\lambda \geq$ 400 nm)	pH n.a.	75% removal (150 min)	[156]
Ciprofloxacin (3.8 mg/L)	FeS/Fe_2S_3/zeolite (2.8 g/L)	100 W tungsten lamp	pH = 3.7	87.2% removal (102 min)	[157]
Ciprofloxacin (10 mg/L)	Ag_2O/Ag_2CO_3/MWCNTs (0.5 g/L)	300 W Xe lamp (λ = 420 nm)	pH n.a.	76% removal (60 min)	[158]
Morphine (10 mg/L)	Ag@g-C_3N_4 (0.17 g/L)	Sunlight irradiation	pH = 2	92.5% removal (120 min) 91% TOC decay (180 min)	[159]

Table 2 (*continued*)

Pharmaceutical (concentration)	Catalyst (concentration)	Light source	Operational conditions	Removal and TOC decay	Ref.
Atenolol (10 mg/L)	$Na_4W_{10}O_{32}$-silica (5 g/L)	Hg lamp	pH = 6	50% removal (102 min)	[160]
Levofloxacin (10 mg/L)	$Na_4W_{10}O_{32}$-silica (5 g/L)	Hg lamp	pH = 6	50% removal (94 min)	[160]
Trimethoprim (10 mg/L)	$Na_4W_{10}O_{32}$-silica (5 g/L)	Hg lamp	pH = 6	50% removal (124 min)	[160]
Levofloxacin (10 mg/L)	Ag/AgBr/BiOBr (1 g/L)	85 W CFL bulb (λ = 450–650 nm)	pH = 8	74% removal (90 min)	[161]
17 α-methyltestosterone (20 mg/L)	Sm (0.3%)/TiO_2 (0.5 mg/L)	1500 W Xe lamp (λ = 300–800 nm)	pH n.a.	82% TOC decay (180 min)	[162]
Ibuprofen (15 mg/L)	Au/meso-TiO_2 (0.5 g/L)	300 W Xe lamp	pH = 5	100% removal (60 min) 95% TOC decay (360 min)	[163]
Carboplatin (20 mg/L)	TiO_2 (0.5 g/L)	9 W UV-A lamp (λ = 340–400 nm)	pH = 6.1	72% removal (30 min) 81% TOC decay (60 min)	[164]
Levofloxacin (10 mg/L)	Bi_3O_4Cl/BiOCl (1 g/L)	85 W CFL bulb (λ = 450–650 nm)	pH = 11	87% removal (180 min) 55% TOC decay (180 min)	[165]
Ofloxacin (10 mg/L)	Bi_2MoO_6 (1 g/L)	Sunlight irradiation	pH = 6	71% removal (90 min)	[166]
Carbamazepine (50 mg/L)	BiOCl/AgCl (1 g/L)	300 W Xe lamp	pH n.a.	79.4% removal (180 min)	[167]
Norfloxacin (10 mg/L)	$FeVO_4$/Fe_2TiO_5 (1 g/L)	500 W Xe lamp	pH n.a.	92% removal (60 min)	[168]
Ibuprofen (40 mg/L)	ZnO (1.5 g/L)	UV lamp	pH n.a.	94.5% removal (120 min)	[169]
Naproxen (40 mg/L)	ZnO (1 g/L)	UV lamp	pH n.a.	98.7% removal (120 min)	[169]
Levofloxacin (10 mg/L)	Bi_2WO_6/CQDs/TiO_2 (0.075 g/L)	Sunlight irradiation	pH = 7	100% removal (90 min)	[170]
Metronidazole (80 mg/L)	TiO_2/Fe^{3+} (0.5 g/L)	125 W UV-C lamp (λ = 247 nm)	pH = 11	97% removal (120 min)	[171]
Carbamazepine (5 mg/L)	$CoFe_2O_4$ (0.2 g/L)	9 W Hg lamp	pH = 2	96% removal (100 min)	[172]
Chloramphenicol (20 mg/L)	attapulgite/Cu_2O/Cu/g-C_3N_4 (0.08 g/L)	300 W Xe lamp	pH = 8.5	61% removal (120 min)	[173]

GO: graphene oxide, NC: clinoptilolite nanoparticles, SDS: sodium dodecyl sulphate, MB: magnetic bentonite, CQDs: carbon quantum dots, mont: montmorillonite, PMS: peroxymonosulfate, CNT: carbon nanotubes, MWCNTs: multi-walled carbon nanotubes.

combining bismuth oxyhalide with metal salts, metal oxides, and noble metals have been developed. BiOX/BiOY (X, Y = Cl, Br, I) exhibit higher photocatalytic activity than single BiOX due to the efficient photoinduced charge separation. However, these promising materials cannot be easily separated and recovered from the aqueous phase, and work is currently underway to develop support matrices. Hu et al. [89] proposed carbon quantum dots (CQDs) as potential supports for BiOCl/BiOBr nanosheet photocatalysts for the removal of tetracycline, attaining 77% after 120 min of treatment. CQDs have been successfully integrated into many semiconductors to prepare hybrid photocatalysts that improve catalytic properties due to their low cost, nontoxicity, facile synthesis, and notable photoelectrochemical properties [90]. Moreover, they can act as electron acceptors and donors; thus, accelerating electron transfer by reducing the recombination of photogenerated charge carriers.

The use of carbon-based nanomaterials for the adsorption of pharmaceutical compounds from water has been extensively reported, with a particular focus on graphene family materials due to the strong π-π interactions between the aromatic ring of graphene and organic molecules. The use of nanostructured carbon with TiO_2 enhances the photocatalytic activity and changes the optical band gap in the visible energy range [91]. According to Zhou et al. [92], the mechanism of action of carbon nanotubes functionalized with TiO_2 involves (1) excitation of an electron from the valence band to the conduction band of the metal oxide, (2) the carbon nanotubes acting as sensitisers transferring electrons to TiO_2, and (3) enhancement of light absorption resulting from the presence of C—O—Ti bond.

3.2. Application of photocatalysis for the removal of pharmaceutical compounds

3.2.1. Antibiotics

Fluoroquinolones, including ciprofloxacin, are commonly prescribed due to their broad-spectrum antibacterial activity. However, due to low absorption, more than 75% of the drug is excreted by humans into wastewater. For this reason, ciprofloxacin was included in the list of top ten pharmaceutical contaminants in aquatic ecosystems [93]. The use of
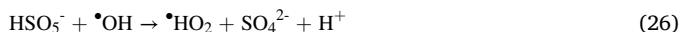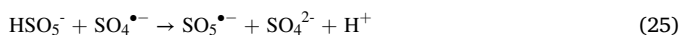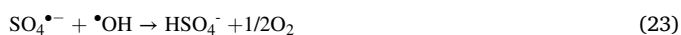
photocatalysis to remove ciprofloxacin has been widely studied. Xia et al. [94] described a novel one-step strategy for the synthesis of CQDs/BiOX (X = Cl, Br, I) in an ionic liquid and reported the complete removal of ciprofloxacin from aqueous solutions after 240 min. The photocatalytic performance of CQDs/BiOBr was attributed to their excellent optical absorption, higher charge separation efficiency and low contact resistance. Moreover, the performance of BiOBr was improved by Fu et al. [95], who prepared a flower-like WS_2/BiOBr heterostructure by hydrothermal one-pot method attaining 83% ciprofloxacin removal. Similarly, the WS_2 heterojunction-based materials were reported to exhibit excellent photocatalytic activity due to the high photon conversion rate and accelerated electron transport. The solution pH plays a key role in the electrostatic attraction/repulsion of the photocatalyst surface and the pollutant molecule, and the zwitterionic property of ciprofloxacin at neutral pH increases the effectiveness of the process [96]. Interference and decreased activity were found in the presence of inorganic environmental matrix compounds. Rashid et al. [93] evaluated butterfly clusters such as a lamellar BiOBr/TiO_2 nanocomposite for the ciprofloxacin removal under visible and solar irradiation, and defluorination of the piperazinyl ring and cleavage of carboxyl groups were found to be the mechanism of action, which is consistent with other studies [97].

Kim and Kan [98] evaluated biochar-based TiO_2 for the degradation of sulfamethoxazole, attaining 75% removal after 180 min of treatment. The synthesised photocatalyst showed higher adsorption capacity compared to commercial TiO_2 powder due to the hydrophobic π-π interactions between the pollutant and the biochar support. They concluded that the presence of inorganic carbon (carbonate and bicarbonate) increases the efficiency of the process, also increasing the toxicity. Makropoulou et al. [99] studied the degradation of sulfamethoxazole using a ZnO-based photocatalyst synthesised by a hydrothermally-assisted method and found an 84% removal after 60 min, under optimal conditions. They attributed the high removal rate to the nanostructured nature of the material, which has a higher relative concentration of lattice defects (oxygen vacancies) that increase charge transport and process efficiency. However, the method reduced the

active surface area of the catalyst, with SEM images showing the formation of nanorods from the original nanoparticles. A WO$_3$-CNT composite was prepared by Zhu et al. [100], who investigated the degradation of sulfamethoxazole under visible-light irradiation. The attack of reactive oxygen species on the benzene/isoxazole ring produced hydroxylated derivatives, which were further oxidised to achieve almost total mineralisation. Cai and Hu [101] proposed the use of a continuous LED/UVA/TiO$_2$ photocatalytic system for the simultaneous degradation of sulfamethoxazole and trimethoprim (400 ppb each pollutant) reporting high removal efficiency.

Heterogeneous photocatalysts have exhibited high degradation and mineralisation of second- and third-generation antibiotics, including tetracycline, cephalosporin, and vancomycin [86]. Tetracyclines have been identified as priority water pollutants by many state environmental agencies due to their potential biotoxicity and low biodegradability [102]. Guo et al. [103] synthesised a 3D Z-scheme based α-FeOOH/FeS$_2$ photocatalyst by a hydrothermal one-pot method for the removal of tetracycline. X-ray spectrometry results confirmed that the original Fe—O—Fe bond was replaced by Fe-S-Fe, which was responsible for the observed enhanced photocatalytic activity, as previously reported by Moradi et al. [104]. Furthermore, the acicular structure of α-FeOOH nanorods seen in microscopic images of TEM prevented aggregation. A complex AgBr/TiO$_2$/palygorskite photocatalyst was developed by Shi et al. [87], who reported 86.67% removal of tetracycline after 90 min of treatment. The amphoteric nature of the compound with three forms at different pHs (protonated form (pH $<$ 4), neutral form (pH = 4–7.5) and monoanionic form (pH = 7.5–10) [105]) presents a challenge in determining the optimal pH for degradation. Although the synthesis of the photocatalyst is complicated, the material was stable and efficient after five consecutive experiments with negligible metal leaching in the main solution.

Liu et al. [106] prepared g-C$_3$N$_4$ @Bi/BiOBr composites based on a ternary structure by a solvothermal method for tetracycline, attaining 78% degradation. Bi/BiOBr nanoplatelets were entrapped on g-C$_3$N$_4$ layers, resulting in the formation of a three-dimensional fluffy hierarchical structure. Photocurrent techniques showed the addition of Bi promoted charge transfer and inhibited the recombination of photoexcited carriers. Based on the band energy potentials and trapping experiments, an indirect Z-scheme system using Bi as an electron-conduction bridge was proposed. Similar results were obtained by Ma et al. [102], who reported high efficiency using g-C$_3$N$_4$ @BiOBr as a photocatalyst for the degradation of tetracycline. Chen et al. [105] developed a coupled oxidation system by integrating photocatalysis and a peroxymonosulfate treatment. This approach can generate a range of oxidising species (Eqs. (21)–(23)), including strong hydroxyl and sulphate radicals and less reactive oxidants such as SO$_5$$^{\bullet-}$ and $^{\bullet}$HO$_2$ (Eqs. (24)–(27)).
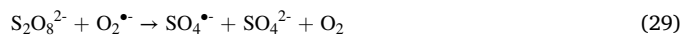
$$SO_4^{\bullet-} + SO_4^{\bullet-} \rightarrow S_2O_8^{2-} \tag{21}$$

$$^{\bullet}OH + {}^{\bullet}OH \rightarrow H_2O_2 \tag{22}$$

$$SO_4^{\bullet-} + {}^{\bullet}OH \rightarrow HSO_4^{-} + 1/2O_2 \tag{23}$$

$$HSO_5^{-} + {}^{\bullet}OH \rightarrow SO_5^{\bullet-} + OH^{-} \tag{24}$$

$$HSO_5^{-} + SO_4^{\bullet-} \rightarrow SO_5^{\bullet-} + SO_4^{2-} + H^{+} \tag{25}$$

$$HSO_5^{-} + {}^{\bullet}OH \rightarrow {}^{\bullet}HO_2 + SO_4^{2-} + H^{+} \tag{26}$$

$$HSO_5^{-} + SO_4^{\bullet-} + H_2O \rightarrow {}^{\bullet}HO_2 + 2SO_4^{2-} + 2H^{+} \tag{27}$$

3.2.2. NSAIDs

The remediation of ibuprofen was studied by Liang et al. [90], who developed a Z-scheme g-C$_3$N$_4$/CQDs/CdIn$_2$S$_4$ composite exhibiting 91% removal after 60 min under visible-light irradiation. Based on the diffuse reflectance results in the ultraviolet/visible region, they found the CQDs

significantly enhanced the absorption of visible light. Photocurrent responses and photoluminescence spectroscopy revealed improved separation efficiency of the photoinduced electron/hole pairs due to the incorporation of CQDs and g-C$_3$N$_4$. However, shielding effects due to the surface of g-C$_3$N$_4$ prevented optimal absorption of incident light. Jallouli et al. [107] investigated a TiO$_2$ - LED irradiated system for the removal of ibuprofen from ultrapure water, municipal wastewater and pharmaceutical industry effluents. As expected, the presence of dissolved organics such as sulphates and carbonates in the main solution contributed to lower degradation of ibuprofen as they compete for active sites and/or reacting species. Analysis of treated effluent samples using the Microtox® test confirmed the photocatalytic system effectively reduced toxicity as a function of increasing mineralisation. The photocatalytic degradation of diclofenac was evaluated by Boukhatem et al. [108], who tested mont-La (6%)-Cu$_{0.6}$Cd$_{0.4}$S as a photocatalyst, achieving 67% TOC decay after 240 min of treatment. While the catalyst showed activity, the system was purged with argon gas. A high oxygen concentration reduces the recombination of photogenerated electrons and increases the production of reactive oxygen species such as HO$^{\bullet}$, O$_2$$^{\bullet-}$ and HO$_2$$^{\bullet}$.

Mu et al. [109] prepared an anatase-TiO$_2$ nanowire composite loaded with Bi$_4$O$_5$I$_2$ by an in-situ calcination method for acetaminophen degradation. Characterisation showed the successful formation of the heterojunction structure on the TiO$_2$ nanowires, and the Bi$_4$O$_5$I$_2$ formed a flower-like morphology as the nanosheets overlapped. Electrochemical impedance spectral analysis confirmed the low charge transfer resistance of the structure. Yan et al. [110] synthesised an In$_2$S$_3$/Zn$_2$GeO$_4$ composite photocatalyst by a hydrothermal co-precipitation method and investigated its effectiveness in the degradation of paracetamol. The remarkable activity was attributed to the photosensitisation of the Zn$_2$GeO$_4$ component by In$_2$S$_3$, which enhanced the absorption of visible-light, with the heterojunction promoting the transfer and separation of photo-induced charge carriers. Mechanistic studies confirmed the role of both holes and superoxide radicals in the photodegradation process, and the influence of solution pH was observed, with electrostatic interactions at pH values $>$ pKa reducing the adsorption of paracetamol. Wang et al. [111] observed synergy and enhanced degradation of paracetamol by a co-oxidation process using BiOCl as a photocatalyst with Na$_2$S$_2$O$_8$ or H$_2$O$_2$. Direct photolysis of S$_2$O$_8$$^{2-}$ resulted in the formation of sulphate radicals by trapping photogenerated electrons (Eq. (28)) and by reaction with O$_2$$^{\bullet-}$ (Eq. (29)). Similar processes were observed by Nezar and Laoufi [112], who used electron acceptors such as H$_2$O$_2$, Na$_2$S$_2$O$_8$ and K$_2$S$_2$O$_8$ to enhance the photocatalytic degradation of metformin.

$$S_2O_8^{2-} + e^{-} \rightarrow SO_4^{\bullet-} + SO_4^{2-} \tag{28}$$

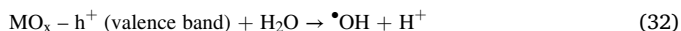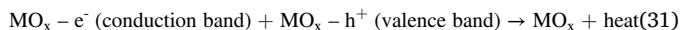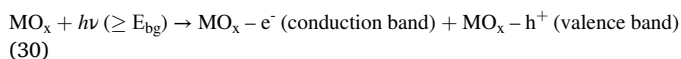$$S_2O_8^{2-} + O_2^{\bullet-} \rightarrow SO_4^{\bullet-} + SO_4^{2-} + O_2 \tag{29}$$

Photocatalytic degradation of ketoprofen was analysed by Djouadi et al. [113], using Bi$_2$S$_3$/TiO$_2$–montmorillonite composites prepared by two-step ion exchange followed by impregnation. At a pH 11, almost total degradation of the parent compound was observed after 120 min of treatment. However, the recalcitrant nature of the by-products from decarboxylation, hydroxylation and further oxidation resulted in low mineralisation (about 10% after 120 min).

4. Photoelectrocatalysis

Photoelectrocatalysis has been shown to be a powerful AOP, enhancing photocatalysis processes by electrochemical bias [114]. The underlying technology is still based on the generation of reactive oxygen species by redox reactions resulting from the adsorption of photons with energy greater than or equal to the band gap of the semiconductor (MO$_x$) (Eq. (30)). To prevent rapid recombination of photon-generated charges (Eq. (31)), a small electrochemical bias can be applied to the system to transport electrons to the separate cathode, where significant additional amounts of the reactive oxygen species can be generated, increasing the

efficiency of the process for water purification – effectively separating the reduction and oxidation reactions (Eq. (32)) [115].
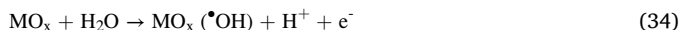
$$MO_x + h\nu (\geq E_{bg}) \rightarrow MO_x - e^- \text{ (conduction band)} + MO_x - h^+ \text{ (valence band)} \quad (30)$$

$$MO_x - e^- \text{ (conduction band)} + MO_x - h^+ \text{ (valence band)} \rightarrow MO_x + heat \quad (31)$$

$$MO_x - h^+ \text{ (valence band)} + H_2O \rightarrow {}^\bullet OH + H^+ \quad (32)$$

The mechanism of the process associated with n-type semiconductors is shown in Fig. 3. The bending of the energetic bands upon application of an external constant bias potential (E_{anod}) results from the change in the electrochemical potential (the Fermi level) of the semiconductor [116]. In addition, the bending of the bands leads to the formation of a space charge layer or depletion layer, which corresponds to the distance between the photocatalyst surface and the beginning of the flat bands. The space charge layer can be increased by applying an additional applied E_{anod} bias with respect to E_{fb} (flat band potential); however, when the maximum E_{anod} is reached, the reaction kinetics is dominated only by the photon flux [114].

The use of carbonaceous materials for the cathode allows in-situ generation of H_2O_2 via cathodic reduction of dissolved oxygen in the bulk solution (Eq. (33)), which in turn can lead to the continuous generation of hydroxyl radicals (Eq. (2)).

$$O_2 + 2H^+ + 2e^- \rightarrow H_2O_2 \quad (33)$$

As part of this process, there is the possibility of oxidation of organic impurities by surface-bound hydroxyl groups on the photoanode (Eq. (34)). However, the low current density (typically below 10 mA·cm^{-2}) results in a low concentration of adsorbed hydroxyl radicals and negligible mineralisation by this route.

$$MO_x + H_2O \rightarrow MO_x ({}^\bullet OH) + H^+ + e^- \quad (34)$$

In addition to the morphology and structure of the photoanode, operating parameters such as the electric potential, irradiation range, applied intensity, electrolyte concentration, solution pH and initial pollutant concentration can also affect the oxidation power and efficiency of the photoelectrochemical process. The applied potential depends primarily on the thickness of the photoanode [117], with a

positive bias driving the separation of electrons and holes, increasing the likelihood of effective oxidation and the generation of reactive oxygen species for direct oxidation. The optimal pH and pKa of the pollutant could enhance the interaction of the pollutant with the photocatalyst. In addition, the addition of sodium sulphate as an electrolyte can minimise the solution resistance to maximise the anodic current density for a given E_{anod}, while the dissolved oxygen in the main solution acts as an electron acceptor and prevents the recombination of the photogenerated electron/hole pairs.

4.1. Common photoanode materials

The search for new materials for photoanodes has recently attracted special attention [114], and the criteria for good candidates are based on the following: (i) light absorption properties and electronic band structures, (ii) oxidation/reduction rate at the surface via photogenerated electron/hole pairs, and (iii) recombination rate of photogenerated charges. The anatase phase of TiO_2 has been extensively used as a photoanode material due to its relatively low cost, negligible toxicity, high chemical stability, and wide band gap (~3.2 eV). Several n-type semiconductors such as WO_3 (E_g = 3.8. eV) and ZnO (E_g = 3.4. eV) have also been successfully used for water treatment. To overcome the photocorrosion problems associated with the use of ZnO, stable heterojunctions have been proposed to enhance the photogenerated charge separation. Changanaqui et al. [118] evaluated the use of $ZnO/TiO_2/Ag_2Se$ to remove oxytetracycline, and achieved 96.5% reduction after 360 min of treatment. The system was able to utilise visible light through the confinement of Ag_2Se (E_{bg} = 1.8 eV) with the ZnO/TiO_2 heterojunction providing a redox potential. A similar approach was taken by Cheng et al. [119], who developed a p-n heterojunction film of Cu_2O/α-Fe_2O_3 for the photoelectrocatalytic degradation of oxytetracycline achieving more than 70% pollutant reduction after 60 min. Composites composed of a p-n heterojunction greatly enhance the transfer of photogenerated holes and promote the separation of photoinduced charge carriers. An example of a commonly used p-type material is Bi_2O_3 due to its negative conduction band and positive valence band edge positions [120].

Relevant publications on pharmaceutical mineralisation by photoelectrocatalysis are summarised in Table 3. Many publications focus on
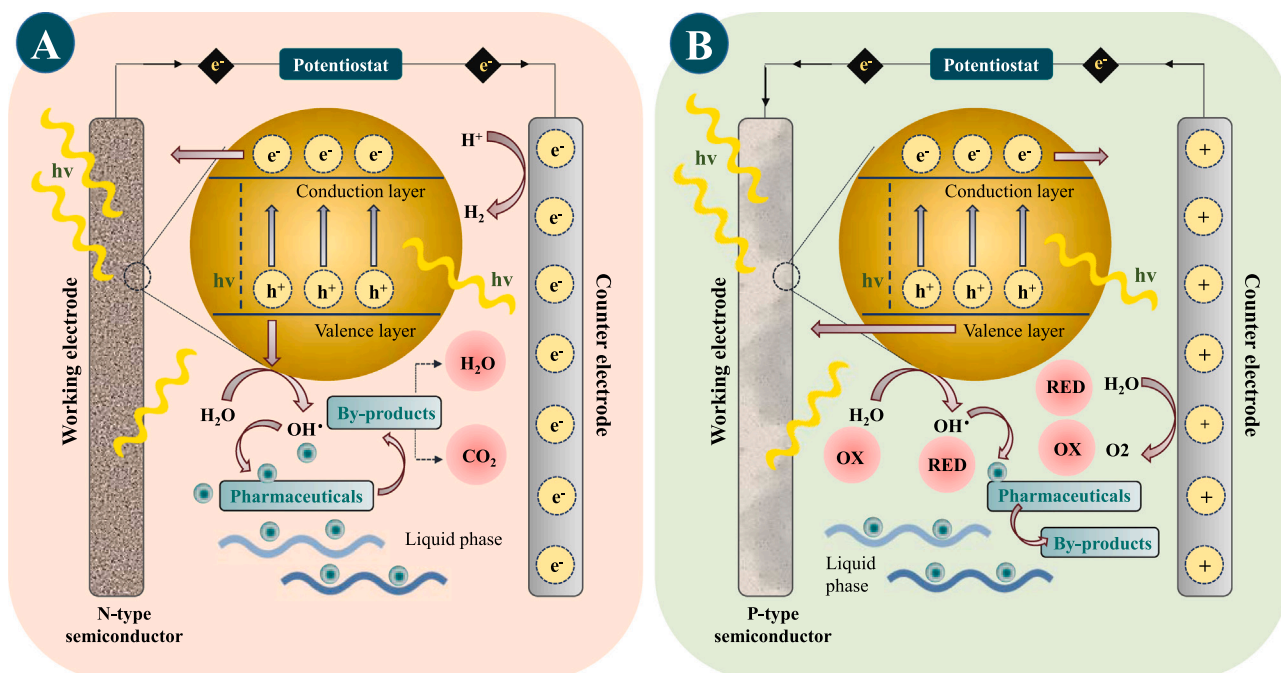

Fig. 3. Mechanism of photoelectrocatalysis detailed the main reactions for (A) n-type semiconductor and (B) p-type semiconductor.

Table 3

Summary of some relevant studies on photoelectrocatalytic systems.

Photoanode	Electrolytic cell	Light source	Pollutant (concentration)	Degradation (time)	Ref.
Ti/TiO$_2$(NT)	Three electrode system: Pt mesh and Ag/AgCl as counter and reference electrode, respectively	150 W Xe lamp (λ = 330–380 nm)	5-fluorouracil (5 mg/L)	100% (150 min)	[117]
ZnO/TiO$_2$/Ag$_2$Se	Three electrode system: Pt wire and Ag/AgCl as counter and reference electrodes, respectively	36 W blue LED lamp (λ = 450–460 nm)	Oxytetracycline (5 mg/L)	96.5% (360 min)	[118]
Cu$_2$O/α-Fe$_2$O$_3$	Three electrode system: Pt wire and Ag/AgCl as counter and reference electrodes, respectively	300 W Xe lamp ($\lambda \geq$ 420 nm)	Oxytetracycline (10 mg/L)	73.3% (60 min)	[119]
Bi$_2$O$_3$/WO$_3$	Three electrode system: Pt wire and SCE as counter and reference electrode, respectively	300 W Xe lamp ($\lambda \geq$ 420 nm)	Norfloxacin (10 mg/L)	88.4% (360 min)	[120]
ZIF-8/NF-TiO$_2$	Three electrode system: Cu sheet and Ag/AgCl as counter and reference electrodes, respectively	300 W Xe lamp ($\lambda \geq$ 420 nm)	Sulfamethazine (10 mg/L)	81.3% (180 min)	[121]
BiVO$_4$/g-C$_3$N$_4$	Three electrode system: Pt wire and SCE as counter and reference electrode, respectively	Xe lamp ($\lambda \geq$ 420 nm)	Diclofenac sodium (10 mg/L)	30.1% (120 min)	[122]
TiO$_2$/Au/TiO$_2$	Three electrode system: rolled Pt thread and Ag/AgCl as counter and reference electrode, respectively	36 W LED UVA lamp (λ = 450–460 nm)	Paracetamol (39 mg/L)	95% (120 min)	[124]
α-Fe$_2$O$_3$/CeO$_2$	Three electrode system: Pt foil and Ag/AgCl as counter and reference electrode, respectively	300 W Xe lamp	Tetracycline hydrochloride (30 mg/L)	88.6% (60 min)	[126]
BiVO$_4$/WO$_3$	Three electrode system: Pt plate and SCE as counter and reference electrode, respectively	300 W Xe lamp ($\lambda \geq$ 420 nm)	Norfloxacin (10 mg/L)	67% (180 min)	[127]
BiVO4/Ag$_3$PO$_4$	Three electrode system: Pt wire and SCE as counter and reference electrode, respectively	300 W Xe lamp ($\lambda \geq$ 420 nm)	Norfloxacin (5 mg/L)	100% (90 min)	[128]
BiVO$_4$/WO$_3$	Three electrode system: Pt foil and SCE as counter and reference electrode, respectively	300 W Xe lamp ($\lambda \geq$ 420 nm)	Levofloxacin (10 mg/L)	60% (300 min)	[129]
BiVO$_4$/WO$_3$	Three electrode system: Pt foil and SCE as counter and reference electrode, respectively	300 W Xe lamp ($\lambda \geq$ 420 nm)	Ketoprofen (10 mg/L)	80% (300 min)	[129]
FTO-BiVO$_4$	Three electrode system: polydopamine modified carbon felt as counter electrode and Ag/AgCl as reference electrode	300 W Xe lamp ($\lambda \geq$ 420 nm)	Ofloxacin (8 mg/L)	99.3% (120 min)	[130]
BiVO$_4$/BiOI	Three electrode system: Pt sheet and Ag/AgCl as counter and reference electrode, respectively	100 W Xe lamp ($\lambda \geq$ 420 nm)	Ciprofloxacin (10 mg/L)	62% (120 min)	[132]
BiVO$_4$/BiOI	Three electrode system: Pt sheet and Ag/AgCl as counter and reference electrode, respectively	100 W Xe lamp ($\lambda \geq$ 420 nm)	Acetaminophen (10 mg/L)	68% (120 min)	[132]
BiVO$_4$/MnO$_2$	Three electrode system: Pt sheet and Ag/AgCl as counter and reference electrodes, respectively	100 W Xe lamp ($\lambda \geq$ 420 nm)	Ciprofloxacin (10 mg/L)	76% (120 min)	[174]
BiWO$_4$/WO$_3$	Three electrode system: Pt foil and SCE as counter and reference electrode, respectively	300 W Xe lamp ($\lambda \geq$ 420 nm)	Tetracycline hydrochloride (10 mg/L)	76.1% (180 min)	[175]
BiVO$_4$/Ag$_2$S	Three electrode system: Pt sheet and Ag/AgCl as counter and reference electrode, respectively	100 W Xe lamp ($\lambda \geq$ 420 nm)	Ciprofloxacin (10 mg/L)	80% (120 min)	[176]
BiVO$_4$/Ag$_2$S	Three electrode system: Pt sheet and Ag/AgCl as counter and reference electrodes, respectively	100 W Xe lamp ($\lambda \geq$ 420 nm)	Sulfamethoxazole (10 mg/L)	86% (120 min)	[176]
BiVO$_4$/TiO$_2$	Three electrode system with Cu$_2$O/TiO$_2$ cathode	300 W Xe lamp ($\lambda \geq$ 420 nm)	Tetracycline hydrochloride (10 mg/L)	30.5% (120 min)	[177]
Sb-doped Sn$_{80\%}$-W$_{20\%}$-oxide	Three electrode system: stainless steel plate and Ag/AgCl as counter and reference electrode, respectively	10 W UVA lamp (λ < 254 nm)	Carbamazepine (0.2 mg/L)	100% (60 min)	[178]

materials chemistry approaches to develop strategies to enhance oxidising power by (i) fabrication of TiO$_2$-based nanostructures, including nanotubes, nanotube arrays, and nanorods, etc [118], (ii) metal doping or non-metal doping (second generation photocatalyst) [121] (iii) synthesis of carbon-based materials (carbon cloth, graphene…) [122], and (iv) the development of tertiary oxides and double perovskites (third generation photocatalyst) [123].

The formation of immobilised nanotube arrays offers significant potential for increasing the electrochemically active surface area. While metal doping of titania with transition metals such as Cr, Co, and Fe can increase recombination and thermal instability, the formation of stable heterostructures can successfully shift the Fermi level. Noble metals can also act as additional electron sinks by promoting electron transfer from the conduction band to the metal, decreasing recombination, and improving quantum yield [124]. Furthermore, these metals often take advantage of the surface plasmon resonance effect that occurs in visible light. For example, Alvaro et al. [125] reported that visible light at 560 nm (near the surface plasmon resonance) can excite nanoparticle gold electrons from gold, enabling transfer to the conduction band of TiO$_2$.

4.2. Application of photoelectrocatalysis to remove pharmaceutical compounds

4.2.1. Antibiotics

Tetracycline is a widely studied contaminant because the compound is toxic and has mutagenic, carcinogenic, and endocrine properties [118]. Cheng et al. [119] developed a p-n heterojunction anode composed of Cu$_2$O/α-Fe$_2$O$_3$ by a two-step deposition process. This material achieved 73% removal of tetracycline after 60 min of photoelectrocatalytic treatment. Analysis of the EIS spectra revealed a low charge transfer resistance, confirming rapid electron transfer at the interface of the p-n heterojunction. In addition, a decrease in the spectral intensity of the photoluminescence compared to the corresponding films of single metal oxides indicates the incorporation of CuO inhibits the recombination of charge carriers. Changanaqui et al. [118] studied the oxytetracycline degradation on nanostructured ZnO/TiO$_2$/Ag$_2$Se photoanodes. The presence of vertically grown hexagonal nanorods and spherical nanoparticles (Ag$_2$Se and residual Ag) adhering to the walls was confirmed by SEM. To ensure photostability, the TiO$_2$ layers were used to protect the ZnO, resulting in excellent reproducibility of the system, as demonstrated by ten consecutive experiments with no visible loss of activity. Similarly, He et al. [126] evaluated a core-shell photocatalyst with direct Z-scheme heterojunction based on α-Fe$_2$O$_3$ nanoparticle layers on CeO$_2$ nanotube arrays and reported high

mineralisation of tetracycline hydrochloride. Jiang et al. [120] studied the removal of the quinolone norfloxacin using synthesised Bi_2O_3/WO_3 p-n heterojunction films, prepared by a hydrothermal one-pot method. The flower-like microstructures possessed low charge transfer resistance, indicating the heterojunction effectively promoted charge separation and electron transfer at the interface. Using visible light, 88% removal of norfloxacin was attained after 360 min of treatment and the photoelectrocatalytic activity was higher than previous publications using the same photoanode [127]. Modification of base electrodes is a popular method for investigating composite materials. Cao et al. [128] assessed the use of an Ag_3PO_4-modified $BiVO_4$ photoanode reaching 100% removal of norfloxacin after 90 min of treatment. The photocurrent density was notably higher than that of the pure $BiVO_4$ electrode; thus, it was assumed that the Ag_3PO_4 reduced the recombination of charge carriers. Applying a high bias voltage significantly reduced the pollutant degradation, probably due to the increasing O_2 evolution by water splitting. This reminds researchers that the PEC system can be a complex process that needs to be optimised.

Levofloxacin, another fluoroquinolone, was used as a model pollutant by Cristino et al. [129]. They used a $WO_3/BiVO_4$ photoanode prepared by electrochemical deposition. The $BiVO_4$ nanoparticles are located in a dense layer of about 200 nm filling the interstices between the WO_3 particles, as can be seen in the SEM images. In such a configuration, charge carrier generation occurs on the $BiVO_4$ layer, with ultrafast electron transfer to WO_3; however, small amounts of hydroxyl radicals were detected in the trapping experiments. Under optimal conditions, nearly total mineralisation of levofloxacin was achieved. However, the aromatic by-products of a second model pollutant, ketoprofen, were more persistent and remained in the main solution after 16 h of treatment. Wang et al. [130] investigated the removal of ofloxacin in a system using $BiVO_4$ as a photoanode and a polydopamine modified carbon felt as a cathode in the presence of peroxymonosulfate (PMS). Complete pollutant degradation was achieved after 120 min, as activation of PMS by polydopamine enhanced the production of reactive species. Increasing the applied potential enhanced charge separation until the saturation potential was reached [131]. Based on radical quenching analysis, sulphate radicals, singlet oxygen, and hydroxyl radicals were found to play a role in the removal of ofloxacin. Thus, the addition of PMS in combination with photoelectrocatalysis is a promising alternative for the pharmaceutical removal from the aqueous phase.

4.2.2. NSAIDs

The degradation of diclofenac was reported by Sun et al. [122], who tested the use of a $g\text{-}C_3N_4/BiVO_4$ composite photoanode, and attained 30.1% removal after 120 min of treatment. XRD analysis revealed the $g\text{-}C_3N_4/BiVO_4$ resulted in a small monoclinic scheelite crystal, leading to a short running distance for the photogenerated electron-hole pairs and an enhanced response to visible light. Furthermore, under optimal conditions produced by high concentrations of hydroxyl radicals and singlet oxygen, the addition of H_2O_2 enabled an efficiency around 62% after 180 min. At a high H_2O_2 concentration, the parallel scavenging reactions (Eqs. (35) and (36)) dominated, with a decrease in diclofenac degradation.

$$H_2O_2 + {}^\bullet OH \rightarrow H_2O + HO_2 \tag{35}$$

$$H_2O_2 + {}^\bullet OH \rightarrow H_2O + O_2 \tag{36}$$

Olvera-Rodríguez et al. [124] synthesised $TiO_2/Au/TiO_2$ film photoanodes by pulsed laser deposition with paracetamol as the target pollutant. The films consisted of alternating layers with a total thickness around 200 nm, which was expected to optimise the absorption of photons and minimise the recombination of charge carriers. They found the inclusion of gold layers extended the photon absorption into the visible range, and a decrease in the photoluminescence signal indicated a significant reduction in the recombination rate. In the presence of a

mixed sulphate and chlorine matrix, almost total paracetamol degradation was achieved after 360 min. The presence of active chlorine species (Eq. (37)) and hydrolysis to hypochlorous acid (Eq. (38)) enhanced paracetamol degradation. At acidic pH, HClO predominates over dissolved Cl_2 and competes with hydroxyl radicals for the pollutant.

$$2\ Cl^- \rightarrow Cl_{2(aq)} + 2\ e^- \tag{37}$$

$$Cl_{2(aq)} + 2H_2O \rightarrow HClO + Cl^- + H^+ \tag{38}$$
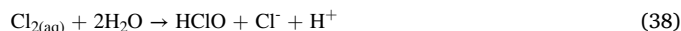
Orimolade et al. [132] also evaluated the degradation of paracetamol using a $BiVO_4/BiOI$ n-p heterojunction system as a photoanode by photoelectrocatalysis driven by visible light. The $BiVO_4$ nanoparticles were successfully entrapped in the flower-like BiOI structures, as shown in the images from SEM. From the photocurrent measurements, they concluded the formation of an n-p heterojunction considerably reduced the recombination rate of the photogenerated electron/hole pairs due to the increased charge transfer at the interface. Further evidence was provided by electrochemical impedance spectroscopy, where the flat band potential was determined via Mott-Schottky plots, which showed a positive slope for $BiVO_4$ and a negative slope for BiOI for the n-type and p-type semiconductors.

5. Conclusions and future perspectives

Pharmaceuticals are recalcitrant organic compounds whose output to the environment is increasingly regulated. This review highlights the growth of academic research aimed at removing these compounds from water through advanced oxidation processes driven by UV energy-including photo-Fenton, photocatalysis and photoelectrocatalysis. A more holistic view of selecting appropriate water treatment technologies requires a more comprehensive understanding of the resulting toxicity of the effluent, the energy required to operate the systems, financial considerations and, perhaps most importantly, how these technologies can be applied at scale. Although there has been progress in the development of new multifunctional materials that offer higher energy absorption, more efficient degradation, and lower toxicity in wastewater streams, more research is needed to ensure industrial-scale applications. There are still a number of knowledge gaps.

1. The use of solar radiation reduces the costs associated with energy use; nevertheless, pilot plants still achieve low pollutant removal compared to laboratory studies. Therefore, further studies are required to increase large-scale economics for real-world applications with large wastewater volumes. In terms of energy consumption, Wardenier et al. [133] reported that 2–3 orders of magnitude higher energy consumption is required to drive UV degradation processes compared to ozonation.
2. Most laboratory-based research studies are conducted with high concentrations of pharmaceuticals (~ 5–50 mg/L), compared to the low concentrations detected in wastewater (likely due to the limitations in analytical chemistry). Thus, initial degradation kinetics appear to be rapid. However, at low pollutant concentrations, the rate constants are much lower, therefore, the behaviour of these technologies should be analysed at lower pollutant concentrations appropriate for the application context.
3. Real effluent is a complex mixture of organic and inorganic compounds – and often difficult to represent in a laboratory setting. The effectiveness of UV-based processes should be evaluated in the presence of organics and other contaminants. Yet few publications test their materials or systems with real wastewater. While we recognise that the contaminant of interest will not always be present, the use of spiked wastewater provides a more realistic test system. The presence of high levels of suspended solids significantly increases turbidity and decreases light intensity due to scattering, reflection, and absorption. In addition, reactive oxygen species are

not selective, so the complexity of the water matrix reduces the efficiency of the process with respect to the compound of interest.

4. Although some studies have been conducted on flow through systems for real industrial wastewater, most of them were carried out at laboratory scale. The dynamic behaviour of the pilot- and full-scale systems should be tested to estimate the operating conditions such as residence time and input flow rate, and to ensure adequate process efficiency to meet the more stringent regulations.

5. There is limited information on the (eco)toxicity of the intermediates generated during the oxidative degradation of drugs using UV-based catalysis.

6. The environmental impact of treatment options should be considered. Although some previous studies have reported promising solar-powered photo-Fenton treatment options even at sites with relatively low solar irradiation [134], additional life-cycle assessment approaches are required to demonstrate the feasibility of environmentally friendly processes.

7. The use of economic parameters that allow evaluation of capital expenditures (CAPEX) and operating expenditures (OPEX) of these processes should be analysed. In addition, the calculation of electrical energy per order (EE/O), which represents the energy required by the system to achieve an order of magnitude reduction in drug concentration per unit volume, would provide a representative parameter that would allow a fair comparison between technologies.

CRediT authorship contribution statement

J. Meijide: Conceptualization, Investigation, Writing – original draft, Writing – review & editing. **G. Lama**: Investigation, Writing – original draft. **M. Pazos**: Funding acquisition, Writing – review & editing. **M.A. Sanromán**: Funding acquisition, Writing – review & editing. **P.S.M. Dunlop**: Writing – review & editing.

Declaration of Competing Interest

The authors declare that they have no known competing financial interests or personal relationships that could have appeared to influence the work reported in this paper.

Acknowledgements

References

[1] X.S. Miao, F. Bishay, M. Chen, C.D. Metcalfe, Occurrence of antimicrobials in the final effluents of wastewater treatment plants in Canada, Environ. Sci. Technol. 38 (2004), https://doi.org/10.1021/es030653q.

[2] D.W. Kolpin, E.T. Furlong, M.T. Meyer, E.M. Thurman, S.D. Zaugg, L.B. Barber, H. T. Buxton, Pharmaceuticals, hormones, and other organic wastewater contaminants in U.S. streams, 1999−2000: a national reconnaissance, Environ. Sci. Technol. 36 (2002) 1202–1211, https://doi.org/10.1021/es011055j.

[3] M. Gros, M. Petrović, A. Ginebreda, D. Barceló, Removal of pharmaceuticals during wastewater treatment and environmental risk assessment using hazard indexes, Environ. Int. 36 (2010) 15–26, https://doi.org/10.1016/J.ENVINT.2009.09.002.

[4] J. Radjenovic, M. Petrovic, D. Barceló, Analysis of pharmaceuticals in wastewater and removal using a membrane bioreactor, Anal. Bioanal. Chem. (2007), https://doi.org/10.1007/s00216-006-0883-6.

[5] B.L. Phoon, C.C. Ong, M.S. Mohamed Saheed, P.L. Show, J.S. Chang, T.C. Ling, S. S. Lam, J.C. Juan, Conventional and emerging technologies for removal of antibiotics from wastewater, J. Hazard. Mater. 400 (2020), https://doi.org/10.1016/j.jhazmat.2020.122961.

[6] C. Farrell, F. Hassard, B. Jefferson, T. Leziart, A. Nocker, P. Jarvis, Turbidity composition and the relationship with microbial attachment and UV inactivation efficacy, Sci. Total Environ. 624 (2018), https://doi.org/10.1016/j.scitotenv.2017.12.173.

[7] F. Biancullo, N.F.F. Moreira, A.R. Ribeiro, C.M. Manaia, J.L. Faria, O.C. Nunes, S. M. Castro-Silva, A.M.T. Silva, Heterogeneous photocatalysis using UVA-LEDs for the removal of antibiotics and antibiotic resistant bacteria from urban wastewater treatment plant effluents, Chem. Eng. J. 367 (2019) 304–313, https://doi.org/10.1016/j.cej.2019.02.012.

[8] J. Sarwar, G. Georgakis, R. LaChance, N. Ozalp, Description and characterization of an adjustable flux solar simulator for solar thermal, thermochemical and photovoltaic applications, Sol. Energy 100 (2014), https://doi.org/10.1016/j.solener.2013.12.008.

[9] M. Tawfik, X. Tonnellier, C. Sansom, Light source selection for a solar simulator for thermal applications: a review, Renew. Sustain. Energy Rev. 90 (2018), https://doi.org/10.1016/j.rser.2018.03.059.

[10] J.J. Pignatello, E. Oliveros, A. MacKay, Advanced oxidation processes for organic contaminant destruction based on the fenton reaction and related chemistry, Crit. Rev. Environ. Sci. Technol. 36 (2006), https://doi.org/10.1080/10643380500326564.

[11] S. Rahim Pouran, A.R. Abdul Aziz, W.M.A. Wan Daud, Review on the main advances in photo-Fenton oxidation system for recalcitrant wastewaters, J. Ind. Eng. Chem. 21 (2015), https://doi.org/10.1016/j.jiec.2014.05.005.

[12] M. Pereira, L. Oliveira, E. Murad, Iron oxide catalysts: Fenton and Fenton-like reactions – a review, Clay Miner. 47 (2012), https://doi.org/10.1180/claymin.2012.047.3.01.

[13] N. Thomas, D.D. Dionysiou, S.C. Pillai, Heterogeneous Fenton catalysts: a review of recent advances, J. Hazard. Mater. 404 (2021), https://doi.org/10.1016/j.jhazmat.2020.124082.

[14] Y. Zhu, R. Zhu, Y. Xi, J. Zhu, G. Zhu, H. He, Strategies for enhancing the heterogeneous Fenton catalytic reactivity: a review, Appl. Catal. B Environ. 255 (2019), https://doi.org/10.1016/j.apcatb.2019.05.041.

[15] Y. Mameri, N. Debbache, M.E.M. Benacherine, N. Seraghni, T. Sehili, Heterogeneous photodegradation of paracetamol using Goethite/H$_2$O$_2$ and Goethite/oxalic acid systems under artificial and natural light, J. Photochem. Photobiol. A Chem. 315 (2016), https://doi.org/10.1016/j.jphotochem.2015.09.019.

[16] J. Gao, S. Wu, Y. Han, F. Tan, Y. Shi, M. Liu, X. Li, 3D mesoporous CuFe$_2$O$_4$ as a catalyst for photo-Fenton removal of sulfonamide antibiotics at near neutral pH, J. Colloid Interface Sci. 524 (2018), https://doi.org/10.1016/j.jcis.2018.03.112.

[17] D. Hermosilla, C. Han, M.N. Nadagouda, L. Machala, A. Gascó, P. Campo, D. D. Dionysiou, Environmentally friendly synthesized and magnetically recoverable designed ferrite photo-catalysts for wastewater treatment applications, J. Hazard. Mater. 381 (2020), https://doi.org/10.1016/j.jhazmat.2019.121200.

[18] C. Lai, F. Huang, G. Zeng, D. Huang, L. Qin, M. Cheng, C. Zhang, B. Li, H. Yi, S. Liu, L. Li, L. Chen, Fabrication of novel magnetic MnFe$_2$O$_4$/bio-char composite and heterogeneous photo-Fenton degradation of tetracycline in near neutral pH, Chemosphere 224 (2019), https://doi.org/10.1016/j.chemosphere.2019.02.193.

[19] Y. Xiang, Y. Huang, B. Xiao, X. Wu, G. Zhang, Magnetic yolk-shell structure of ZnFe2O4 nanoparticles for enhanced visible light photo-Fenton degradation towards antibiotics and mechanism study, Appl. Surf. Sci. 513 (2020), https://doi.org/10.1016/j.apsusc.2020.145820.

[20] Y. Ma, B. Wang, Q. Wang, S. Xing, Facile synthesis of Α-FeOOH/Γ-Fe$_2$O$_3$ by a pH gradient method and the role of Γ-Fe2O3 in H$_2$O$_2$ activation under visible light irradiation, Chem. Eng. J. 354 (2018), https://doi.org/10.1016/j.cej.2018.08.011.

[21] X. Huang, N. Zhu, F. Mao, Y. Ding, S. Zhang, H. Liu, F. Li, P. Wu, Z. Dang, Y. Ke, Enhanced heterogeneous photo-Fenton catalytic degradation of tetracycline over γCeO$_2$/Fh composites: performance, degradation pathways, Fe2+ regeneration and mechanism, Chem. Eng. J. 392 (2020), https://doi.org/10.1016/j.cej.2019.123636.

[22] Q. Jiang, R. Zhu, Y. Zhu, Q. Chen, Efficient degradation of cefotaxime by a UV+ ferrihydrite/TiO2+H2O2 process: the important role of ferrihydrite in transferring photo-generated electrons from TiO$_2$ to H$_2$O$_2$, J. Chem. Technol. Biotechnol. 94 (2019), https://doi.org/10.1002/jctb.6041.

[23] D.J. Perisic, V. Gilja, M.N. Stankov, Z. Katancic, H. Kusic, U.L. Stangar, D. D. Dionysiou, A.L. Bozic, Removal of diclofenac from water by zeolite-assisted advanced oxidation processes, J. Photochem. Photobiol. A Chem. 321 (2016), https://doi.org/10.1016/j.jphotochem.2016.01.030.

[24] L. Hurtado, R. Romero, A. Mendoza, S. Brewer, R. Donkor, R.M. Gómez-Espinosa, R. Natividad, Paracetamol mineralization by Photo Fenton process catalyzed by a Cu/Fe-PILC under circumneutral pH conditions, J. Photochem. Photobiol. A Chem. 373 (2019), https://doi.org/10.1016/j.jphotochem.2019.01.012.

[25] S.T. Khankhasaeva, S.V. Badmaeva, Removal of p-aminobenzenesulfanilamide from water solutions by catalytic photo-oxidation over Fe-pillared clay, Water Res. 185 (2020), https://doi.org/10.1016/j.watres.2020.116212.

[26] X. Cheng, Q. Cheng, X. Deng, P. Wang, H. Liu, A facile and novel strategy to synthesize reduced TiO$_2$ nanotubes photoelectrode for photoelectrocatalytic degradation of diclofenac, Chemosphere 144 (2016), https://doi.org/10.1016/j.chemosphere.2015.09.070.

[27] S. Guo, W. Yang, L. You, J. Li, J. Chen, K. Zhou, Simultaneous reduction of Cr(VI) and degradation of tetracycline hydrochloride by a novel iron-modified rectorite composite through heterogeneous photo-Fenton processes, Chem. Eng. J. 393 (2020), https://doi.org/10.1016/j.cej.2020.124758.

[28] A. Cruz, L. Couto, S. Esplugas, C. Sans, Study of the contribution of homogeneous catalysis on heterogeneous Fe(III)/alginate mediated photo-Fenton process, Chem. Eng. J. 318 (2017), https://doi.org/10.1016/j.cej.2016.09.014.

[29] Z. Du, F. Liu, C. Xiao, Y. Dan, L. Jiang, Fabrication of poly(vinyl alcohol)/sodium alginate hydrogel beads and its application in photo-Fenton degradation of tetracycline, J. Mater. Sci. 56 (2021), https://doi.org/10.1007/s10853-020-05299-7.

[30] M. Nawaz, A. Shahzad, K. Tahir, J. Kim, M. Moztahida, J. Jang, M.B. Alam, S. H. Lee, H.Y. Jung, D.S. Lee, Photo-Fenton reaction for the degradation of sulfamethoxazole using a multi-walled carbon nanotube-NiFe2O4 composite, Chem. Eng. J. 382 (2020), https://doi.org/10.1016/j.cej.2019.123053.

[31] T. Shi, J. Peng, J. Chen, C. Sun, H. He, Heterogeneous photo-Fenton degradation of norfloxacin with Fe3O4-multiwalled carbon nanotubes in aqueous solution, Catal. Lett. 147 (2017), https://doi.org/10.1007/s10562-017-2026-4.

[32] E. Bocos, N. Oturan, M. Pazos, M.Á. Sanromán, M.A. Oturan, Elimination of radiocontrast agent diatrizoic acid by photo-Fenton process and enhanced treatment by coupling with electro-Fenton process, Environ. Sci. Pollut. Res. 23 (2016), https://doi.org/10.1007/s11356-016-7054-x.

[33] B. Kakavandi, A. Takdastan, N. Jaafarzadeh, M. Azizi, A. Mirzaei, A. Azari, Application of Fe3O4@C catalyzing heterogeneous UV-Fenton system for tetracycline removal with a focus on optimization by a response surface method, J. Photochem. Photobiol. A Chem. 314 (2016), https://doi.org/10.1016/j.jphotochem.2015.08.008.

[34] X. Wang, A. Wang, J. Ma, Visible-light-driven photocatalytic removal of antibiotics by newly designed C3N4@MnFe2O4-graphene nanocomposites, J. Hazard. Mater. 336 (2017), https://doi.org/10.1016/j.jhazmat.2017.04.012.

[35] T. Guo, K. Wang, G. Zhang, X. Wu, A novel α-Fe2O3@g-C3N4 catalyst: synthesis derived from Fe-based MOF and its superior photo-Fenton performance, Appl. Surf. Sci. 469 (2019), https://doi.org/10.1016/j.apsusc.2018.10.183.

[36] J. Meijide, P.S.M. Dunlop, M. Pazos, M.A. Sanromán, Heterogeneous electro-fenton as "Green" technology for pharmaceutical removal: a review, Catalysts 11 (2021) 1–22, https://doi.org/10.3390/catal11010085.

[37] X. Wang, R. Yin, L. Zeng, M. Zhu, A review of graphene-based nanomaterials for removal of antibiotics from aqueous environments, Environ. Pollut. 253 (2019), https://doi.org/10.1016/j.envpol.2019.06.067.

[38] X. Wang, X. Zhang, Y. Zhang, Y. Wang, S.P. Sun, W.D. Wu, Z. Wu, Nanostructured semiconductor supported iron catalysts for heterogeneous photo-Fenton oxidation: a review, J. Mater. Chem. A 8 (2020), https://doi.org/10.1039/d0ta04541a.

[39] J. Zhao, M. Ji, J. Di, Y. Zhang, M. He, H. Li, J. Xia, Novel Z-scheme heterogeneous photo-Fenton-like g-C3N4/FeOCl for the pollutants degradation under visible light irradiation, J. Photochem. Photobiol. A Chem. 391 (2020), https://doi.org/10.1016/j.jphotochem.2019.112343.

[40] J. Jiang, X. Wang, Y. Liu, Y. Ma, T. Li, Y. Lin, T. Xie, S. Dong, Photo-Fenton degradation of emerging pollutants over Fe-POM nanoparticle/porous and ultrathin g-C3N4 nanosheet with rich nitrogen defect: degradation mechanism, pathways, and products toxicity assessment, Appl. Catal. B Environ. 278 (2020), https://doi.org/10.1016/j.apcatb.2020.119349.

[41] J. Jiang, J. Gao, T. Li, Y. Chen, Q. Wu, T. Xie, Y. Lin, S. Dong, Visible-light-driven photo-Fenton reaction with α-Fe2O3/BiOI at near neutral pH: boosted photogenerated charge separation, optimum operating parameters and mechanism insight, J. Colloid Interface Sci. 554 (2019), https://doi.org/10.1016/j.jcis.2019.07.038.

[42] Z. Wang, C. Lai, L. Qin, Y. Fu, J. He, D. Huang, B. Li, M. Zhang, S. Liu, L. Li, W. Zhang, H. Yi, X. Liu, X. Zhou, ZIF-8-modified MnFe2O4 with high crystallinity and superior photo-Fenton catalytic activity by Zn-O-Fe structure for TC degradation, Chem. Eng. J. 392 (2020), https://doi.org/10.1016/j.cej.2020.124851.

[43] K.K. Barnes, D.W. Kolpin, E.T. Furlong, S.D. Zaugg, M.T. Meyer, L.B. Barber, A national reconnaissance of pharmaceuticals and other organic wastewater contaminants in the United States - I) groundwater, Sci. Total Environ. 402 (2008), https://doi.org/10.1016/j.scitotenv.2008.04.028.

[44] I.T. Carvalho, L. Santos, Antibiotics in the aquatic environments: a review of the European scenario, Environ. Int. 94 (2016), https://doi.org/10.1016/j.envint.2016.06.025.

[45] C. Tong, X. Zhuo, Y. Guo, Occurrence and risk assessment of four typical fluoroquinolone antibiotics in raw and treated sewage and in receiving waters in Hangzhou, China, J. Agric. Food Chem. 59 (2011), https://doi.org/10.1021/jf2013937.

[46] Y. Xiao, H. Chang, A. Jia, J. Hu, Trace analysis of quinolone and fluoroquinolone antibiotics from wastewaters by liquid chromatography-electrospray tandem mass spectrometry, J. Chromatogr. A 1214 (2008), https://doi.org/10.1016/j.chroma.2008.10.090.

[47] Z. Du, K. Li, S. Zhou, X. Liu, Y. Yu, Y. Zhang, Y. He, Y. Zhang, Degradation of ofloxacin with heterogeneous photo-Fenton catalyzed by biogenic Fe-Mn oxides, Chem. Eng. J. 380 (2020), https://doi.org/10.1016/j.cej.2019.122427.

[48] Y. Tian, X. He, W. Chen, X. Tian, Y. Nie, B. Han, H.M. Lin, C. Yang, Y. Wang, Significant enhancement of photo-Fenton degradation of ofloxacin over Fe-Dis@ Sep due to highly dispersed FeC6 with electron deficiency, Sci. Total Environ. 723 (2020), https://doi.org/10.1016/j.scitotenv.2020.138144.

[49] X. Tian, X. He, Y. Nie, Z. Zhou, C. Yang, Y. Wang, Surface deep oxidation of ofloxacin and 2,4-dichlorophenol over ferrocene@sepiolite due to their synergistic effect in visible light driven heterogeneous Fenton reaction process, Environ. Sci. Nano 5 (2018), https://doi.org/10.1039/c8en00295a.

[50] R. Changotra, H. Rajput, A. Dhir, Natural soil mediated photo Fenton-like processes in treatment of pharmaceuticals: batch and continuous approach, Chemosphere 188 (2017), https://doi.org/10.1016/j.chemosphere.2017.09.016.

[51] M. Hakimi, M. Alikhani, Characterization of α-Fe2O3 nanoparticles prepared from a new [Fe(Ofloxacin)2Cl2] precursor: a heterogeneous photocatalyst for removal of methylene blue and ciprofloxacin in water, J. Inorg. Organomet. Polym. Mater. 30 (2020), https://doi.org/10.1007/s10904-019-01210-3.

[52] J.A. d L. Perini, B.C. e Silva, A.L. Tonetti, R.F.P. Nogueira, Photo-Fenton degradation of the pharmaceuticals ciprofloxacin and fluoxetine after anaerobic pre-treatment of hospital effluent, Environ. Sci. Pollut. Res. 24 (2017) 6233–6240, https://doi.org/10.1007/s11356-016-7416-4.

[53] A. Tacic, V. Nikolic, L. Nikolic, I. Savic, Antimicrobial sulfonamide drugs, Adv. Technol. 6 (2017), https://doi.org/10.5937/savteh1701058t.

[54] Y. Bai, X. Ruan, F. Wang, G. Antoine, J.P. van der Hoek, Sulfonamides removal under different redox conditions and microbial response to sulfonamides stress during riverbank filtration: a laboratory column study, Chemosphere 220 (2019), https://doi.org/10.1016/j.chemosphere.2018.12.167.

[55] Y. Deng, B. Li, T. Zhang, Bacteria that make a meal of sulfonamide antibiotics: blind spots and emerging opportunities, Environ. Sci. Technol. 52 (2018), https://doi.org/10.1021/acs.est.7b06026.

[56] B. Morasch, F. Bonvin, H. Reiser, D. Grandjean, L.F. De Alencastro, C. Perazzolo, N. Chèvre, T. Kohn, Occurrence and fate of micropollutants in the Vidy Bay of Lake Geneva, Switzerland. Part II: Micropollutant removal between wastewater and raw drinking water, Environ. Toxicol. Chem. 29 (2010), https://doi.org/10.1002/etc.222.

[57] F. Bonvin, J. Omlin, R. Rutler, W.B. Schweizer, P.J. Alaimo, T.J. Strathmann, K. McNeill, T. Kohn, Direct photolysis of human metabolites of the antibiotic sulfamethoxazole: evidence for abiotic back-transformation, Environ. Sci. Technol. 47 (2013), https://doi.org/10.1021/es303777k.

[58] M. Al Aukidy, P. Verlicchi, A. Jelic, M. Petrovic, D. Barcelò, Monitoring release of pharmaceutical compounds: occurrence and environmental risk assessment of two WWTP effluents and their receiving bodies in the Po Valley, Italy, Sci. Total Environ. 438 (2012), https://doi.org/10.1016/j.scitotenv.2012.08.061.

[59] A. Serra-Clusellas, L. De Angelis, C.H. Lin, P. Vo, M. Bayati, L. Sumner, Z. Lei, N. B. Amaral, L.M. Bertini, J. Mazza, L.R. Pizzio, J.D. Stripeikis, J.A. Rengifo-Herrera, M.M. Fidalgo de Cortalezzi, Abatement of 2,4-D by H2O2 solar photolysis and solar photo-Fenton-like process with minute Fe(III) concentrations, Water Res. 144 (2018), https://doi.org/10.1016/j.watres.2018.07.072.

[60] Y. Li, B. Zhang, X. Liu, Q. Zhao, H. Zhang, Y. Zhang, P. Ning, S. Tian, Ferrocene-catalyzed heterogeneous Fenton-like degradation mechanisms and pathways of antibiotics under simulated sunlight: a case study of sulfamethoxazole, J. Hazard. Mater. 353 (2018), https://doi.org/10.1016/j.jhazmat.2018.02.034.

[61] Y. Ji, Y. Fan, K. Liu, D. Kong, J. Lu, Thermo activated persulfate oxidation of antibiotic sulfamethoxazole and structurally related compounds, Water Res. 87 (2015), https://doi.org/10.1016/j.watres.2015.09.005.

[62] H. Tian, J. Peng, Q. Du, X. Hui, H. He, One-pot sustainable synthesis of magnetic MIL-100(Fe) with novel Fe3O4 morphology and its application in heterogeneous degradation, Dalton Trans. 47 (2018), https://doi.org/10.1039/c7dt04819j.

[63] M. Cheng, Y. Liu, D. Huang, C. Lai, G. Zeng, J. Huang, Z. Liu, C. Zhang, C. Zhou, L. Qin, W. Xiong, H. Yi, Y. Yang, Prussian blue analogue derived magnetic Cu-Fe oxide as a recyclable photo-Fenton catalyst for the efficient removal of sulfamethazine at near neutral pH values, Chem. Eng. J. 362 (2019), https://doi.org/10.1016/j.cej.2019.01.101.

[64] I. Gozlan, A. Rotstein, D. Avisar, Amoxicillin-degradation products formed under controlled environmental conditions: identification and determination in the aquatic environment, Chemosphere 91 (2013), https://doi.org/10.1016/j.chemosphere.2013.01.095.

[65] L. Rizzo, S. Meric, M. Guida, D. Kassinos, V. Belgiorno, Heterogenous photocatalytic degradation kinetics and detoxification of an urban wastewater treatment plant effluent contaminated with pharmaceuticals, Water Res. 43 (2009), https://doi.org/10.1016/j.watres.2009.06.046.

[66] D. Fatta-Kassinos, I.K. Kalavrouziotis, P.H. Koukoulakis, M.I. Vasquez, The risks associated with wastewater reuse and xenobiotics in the agroecological environment, Sci. Total Environ. 409 (2011), https://doi.org/10.1016/j.scitotenv.2010.03.036.

[67] J.H. Ramírez-Franco, L.A. Galeano, M.A. Vicente, Fly ash as photo-Fenton catalyst for the degradation of amoxicillin, J. Environ. Chem. Eng. 7 (2019), https://doi.org/10.1016/j.jece.2019.103274.

[68] A. Garcia-Rodríguez, V. Matamoros, C. Fontàs, V. Salvadó, The influence of light exposure, water quality and vegetation on the removal of sulfonamides and tetracyclines: a laboratory-scale study, Chemosphere 90 (2013), https://doi.org/10.1016/j.chemosphere.2012.09.092.

[69] H.M. Jang, E. Kan, A novel hay-derived biochar for removal of tetracyclines in water, Bioresour. Technol. 274 (2019), https://doi.org/10.1016/j.biortech.2018.11.081.

[70] Q. Guo, L. Jing, Y. Lan, M. He, Y. Xu, H. Xu, H. Li, Construction 3D rod-like Bi3.64Mo0.36O6.55/CuBi2O4 photocatalyst for enhanced photocatalytic activity via a photo-Fenton-like Cu2+/Cu+ redox cycle, Sep. Purif. Technol. 254 (2021), https://doi.org/10.1016/j.seppur.2020.117546.

[71] S. Dahane, M.D. Gil García, M.J. Martínez Bueno, A. Uclés Moreno, M. Martínez Galera, A. Derdour, Determination of drugs in river and wastewaters using solid-phase extraction by packed multi-walled carbon nanotubes and liquid chromatography-quadrupole-linear ion trap-mass spectrometry, J. Chromatogr. A 1297 (2013), https://doi.org/10.1016/j.chroma.2013.05.002.

[72] N. Larsson, E. Petersson, M. Rylander, J.Å. Jönsson, Continuous flow hollow fiber liquid-phase microextraction and monitoring of NSAID pharmaceuticals in a sewage treatment plant effluent, Anal. Methods 1 (2009), https://doi.org/10.1039/b9ay00015a.

[73] V. Koutsouba, T. Heberer, B. Fuhrmann, K. Schmidt-Baumler, D. Tsipi, A. Hiskia, Determination of polar pharmaceuticals in sewage water of Greece by gas

chromatography-mass spectrometry, Chemosphere 51 (2003), https://doi.org/10.1016/S0045-6535(02)00819-6.

[74] L.A. Pérez-Estrada, M.I. Maldonado, W. Gernjak, A. Agüera, A.R. Fernández-Alba, M.M. Ballesteros, S. Malato, Decomposition of diclofenac by solar driven photocatalysis at pilot plant scale, Catal. Today (2005), https://doi.org/10.1016/j.cattod.2005.03.013.

[75] B. Manu, Degradation kinetics of diclofenac in water by Fenton's oxidation, J. Sustain. Energy Environ. 3 (2012).

[76] J. Xu, Y. Li, B. Yuan, C. Shen, M. Fu, H. Cui, W. Sun, Large scale preparation of Cu-doped α-FeOOH nanoflowers and their photo-Fenton-like catalytic degradation of diclofenac sodium, Chem. Eng. J. 291 (2016), https://doi.org/10.1016/j.cej.2016.01.059.

[77] S.Y. Arzate-Salgado, A.A. Morales-Pérez, M. Solís-López, R.M. Ramírez-Zamora, Evaluation of metallurgical slag as a Fenton-type photocatalyst for the degradation of an emerging pollutant: diclofenac, Catal. Today (2016), https://doi.org/10.1016/j.cattod.2015.09.026.

[78] C.B. Molina, E. Sanz-Santos, A. Boukhemkhem, J. Bedia, C. Belver, J.J. Rodriguez, Removal of emerging pollutants in aqueous phase by heterogeneous Fenton and photo-Fenton with Fe2O3-TiO2-clay heterostructures, Environ. Sci. Pollut. Res. 27 (2020), https://doi.org/10.1007/s11356-020-09236-8.

[79] T.A. Ternes, Occurrence of drugs in German sewage treatment plants and rivers, Water Res. 32 (1998), https://doi.org/10.1016/S0043-1354(98)00099-2.

[80] P.H. Roberts, K.V. Thomas, The occurrence of selected pharmaceuticals in wastewater effluent and surface waters of the lower Tyne catchment, Sci. Total Environ. 356 (2006), https://doi.org/10.1016/j.scitotenv.2005.04.031.

[81] N. El-Gendy, K.L. Aillon, C. Berkland, Dry powdered aerosols of diatrizoic acid nanoparticle agglomerates as a lung contrast agent, Int. J. Pharm. 391 (2010), https://doi.org/10.1016/j.ijpharm.2010.03.009.

[82] S. Allard, J. Criquet, A. Prunier, C. Falantin, A. Le Person, J. Yat-Man Tang, J. P. Croué, Photodecomposition of iodinated contrast media and subsequent formation of toxic iodinated moieties during final disinfection with chlorinated oxidants, Water Res. 103 (2016), https://doi.org/10.1016/j.watres.2016.07.050.

[83] T. Rastogi, C. Leder, K. Kümmerer, Qualitative environmental risk assessment of photolytic transformation products of iodinated X-ray contrast agent diatrizoic acid, Sci. Total Environ. (2014) 482–483, https://doi.org/10.1016/j.scitotenv.2014.02.139.

[84] M. Pelaez, N.T. Nolan, S.C. Pillai, M.K. Seery, P. Falaras, A.G. Kontos, P.S. M. Dunlop, J.W.J. Hamilton, J.A. Byrne, K. O'Shea, M.H. Entezari, D. D. Dionysiou, A review on the visible light active titanium dioxide photocatalysts for environmental applications, Appl. Catal. B Environ. 125 (2012) 331–349, https://doi.org/10.1016/j.apcatb.2012.05.036.

[85] A.L. Linsebigler, G. Lu, J.T. Yates, Photocatalysis on TiO2 surfaces: principles, mechanisms, and selected results, Chem. Rev. 95 (1995), https://doi.org/10.1021/cr00035a013.

[86] J.C. Durán-Álvarez, E. Avella, R.M. Ramírez-Zamora, R. Zanella, Photocatalytic degradation of ciprofloxacin using mono- (Au, Ag and Cu) and bi- (Au-Ag and Au-Cu) metallic nanoparticles supported on TiO2 under UV-C and simulated sunlight, Catal. Today (2016), https://doi.org/10.1016/j.cattod.2015.07.033.

[87] Y. Shi, Z. Yan, Y. Xu, T. Tian, J. Zhang, J. Pang, X. Peng, Q. Zhang, M. Shao, W. Tan, H. Li, Q. Xiong, Visible-light-driven AgBr–TiO2-palygorskite photocatalyst with excellent photocatalytic activity for tetracycline hydrochloride, J. Clean. Prod. 277 (2020), https://doi.org/10.1016/j.jclepro.2020.124021.

[88] M. Du, Y. Du, Y. Feng, Z. Li, J. Wang, N. Jiang, Y. Liu, Advanced photocatalytic performance of novel BiOBr/BiOI/cellulose composites for the removal of organic pollutant, Cellulose 26 (2019), https://doi.org/10.1007/s10570-019-02474-1.

[89] Q. Hu, M. Ji, J. Di, B. Wang, J. Xia, Y. Zhao, H. Li, Ionic liquid-induced double regulation of carbon quantum dots modified bismuth oxychloride/bismuth oxybromide nanosheets with enhanced visible-light photocatalytic activity, J. Colloid Interface Sci. 519 (2018), https://doi.org/10.1016/j.jcis.2018.02.057.

[90] M. Liang, Z. Zhang, R. Long, Y. Wang, Y. Yu, Y. Pei, Design of a Z-scheme g-C3N4/CQDs/CdIn2S4 composite for efficient visible-light-driven photocatalytic degradation of ibuprofen, Environ. Pollut. 259 (2020), https://doi.org/10.1016/j.envpol.2019.113770.

[91] X. Wang, A. Wang, M. Lu, J. Ma, Synthesis of magnetically recoverable Fe0/graphene-TiO2 nanowires composite for both reduction and photocatalytic oxidation of metronidazole, Chem. Eng. J. 337 (2018), https://doi.org/10.1016/j.cej.2017.12.090.

[92] W. Zhou, K. Pan, Y. Qu, F. Sun, C. Tian, Z. Ren, G. Tian, H. Fu, Photodegradation of organic contamination in wastewaters by bonding TiO2/single-walled carbon nanotube composites with enhanced photocatalytic activity, Chemosphere 81 (2010), https://doi.org/10.1016/j.chemosphere.2010.08.059.

[93] J. Rashid, A. Abbas, L.C. Chang, A. Iqbal, I.U. Haq, A. Rehman, S.U. Awan, M. Arshad, M. Rafique, M.A. Barakat, Butterfly cluster like lamellar BiOBr/TiO2 nanocomposite for enhanced sunlight photocatalytic mineralization of aqueous ciprofloxacin, Sci. Total Environ. 665 (2019), https://doi.org/10.1016/j.scitotenv.2019.02.145.

[94] J. Xia, J. Di, H. Li, H. Xu, H. Li, S. Guo, Ionic liquid-induced strategy for carbon quantum dots/BiOX (X=Br, Cl) hybrid nanosheets with superior visible light-driven photocatalysis, Appl. Catal. B Environ. 181 (2016), https://doi.org/10.1016/j.apcatb.2015.07.035.

[95] S. Fu, X. Liu, Y. Yan, L. Li, H. Liu, F. Zhao, J. Zhou, Few-layer WS2 modified BiOBr nanosheets with enhanced broad-spectrum photocatalytic activity towards various pollutants removal, Sci. Total Environ. 694 (2019), https://doi.org/10.1016/j.scitotenv.2019.133756.

[96] H.G. Guo, N.Y. Gao, W.H. Chu, L. Li, Y.J. Zhang, J.S. Gu, Y.L. Gu, Photochemical degradation of ciprofloxacin in UV and UV/H2O2 process: Kinetics, parameters, and products, Environ. Sci. Pollut. Res. 20 (2013), https://doi.org/10.1007/s11356-012-1229-x.

[97] A. Salma, S. Thöroe-Boveleth, T.C. Schmidt, J. Tuerk, Dependence of transformation product formation on pH during photolytic and photocatalytic degradation of ciprofloxacin, J. Hazard. Mater. 313 (2016), https://doi.org/10.1016/j.jhazmat.2016.03.010.

[98] J.R. Kim, E. Kan, Heterogeneous photocatalytic degradation of sulfamethoxazole in water using a biochar-supported TiO2 photocatalyst, J. Environ. Manag. 180 (2016), https://doi.org/10.1016/j.jenvman.2016.05.016.

[99] T. Makropoulou, I. Kortidis, K. Davididou, D.E. Motaung, E. Chatzisymeon, Photocatalytic facile ZnO nanostructures for the elimination of the antibiotic sulfamethoxazole in water, J. Water Process Eng. 36 (2020), https://doi.org/10.1016/j.jwpe.2020.101299.

[100] W. Zhu, Z. Li, C. He, S. Faqian, Y. Zhou, Enhanced photodegradation of sulfamethoxazole by a novel WO3-CNT composite under visible light irradiation, J. Alloy. Compd. 754 (2018), https://doi.org/10.1016/j.jallcom.2018.04.286.

[101] Q. Cai, J. Hu, Decomposition of sulfamethoxazole and trimethoprim by continuous UVA/LED/TiO2 photocatalysis: decomposition pathways, residual antibacterial activity and toxicity, J. Hazard. Mater. 323 (2017), https://doi.org/10.1016/j.jhazmat.2016.06.006.

[102] Z. Ma, L. Deng, G. Fan, Y. He, Hydrothermal synthesis of p-C3N4/f-BiOBr composites with highly efficient degradation of methylene blue and tetracycline, Spectrochim. Acta Part A Mol. Biomol. Spectrosc. 214 (2019), https://doi.org/10.1016/j.saa.2019.02.008.

[103] Y. Guo, C. Li, Z. Gong, Y. Guo, X. Wang, B. Gao, W. Qin, G. Wang, Photocatalytic decontamination of tetracycline and Cr(VI) by a novel α-FeOOH/FeS2 photocatalyst: one-pot hydrothermal synthesis and Z-scheme reaction mechanism insight, J. Hazard. Mater. 397 (2020), https://doi.org/10.1016/j.jhazmat.2020.122580.

[104] M. Moradi, G. Moussavi, K. Yaghmaeian, A. Yazdanbakhsh, V. Srivastava, M. Sillanpää, Synthesis of novel Ag-doped S-MgO nanosphere as an efficient UVA/LED-activated photocatalyst for non-radical oxidation of diclofenac: catalyst preparation and characterization and photocatalytic mechanistic evaluation, Appl. Catal. B Environ. 260 (2020), https://doi.org/10.1016/j.apcatb.2019.118128.

[105] X. Chen, J. Zhou, Y. Chen, Y. Zhou, L. Ding, H. Liang, X. Li, Degradation of tetracycline hydrochloride by coupling of photocatalysis and peroxymonosulfate oxidation processes using CuO-BiVO4 heterogeneous catalyst, Process Saf. Environ. Prot. 145 (2021), https://doi.org/10.1016/j.psep.2020.08.016.

[106] H. Liu, H. Zhou, X. Liu, H. Li, C. Ren, X. Li, W. Li, Z. Lian, M. Zhang, Engineering design of hierarchical g-C3N4@Bi/BiOBr ternary heterojunction with Z-scheme system for efficient visible-light photocatalytic performance, J. Alloy. Compd. 798 (2019), https://doi.org/10.1016/j.jallcom.2019.05.303.

[107] N. Jallouli, L.M. Pastrana-Martínez, A.R. Ribeiro, N.F.F. Moreira, J.L. Faria, O. Hentati, A.M.T. Silva, M. Ksibi, Heterogeneous photocatalytic degradation of ibuprofen in ultrapure water, municipal and pharmaceutical industry wastewaters using a TiO2/UV-LED system, Chem. Eng. J. 334 (2018) 976–984, https://doi.org/10.1016/j.cej.2017.10.045.

[108] H. Boukhatem, H. Khalaf, L. Djouadi, Z. Marin, R.M. Navarro, J.A. Santaballa, M. Canle, Diclofenac degradation using mont-La (6%)-Cu0.6Cd0.4S as photocatalyst under NUV-Vis irradiation. Operational parameters, kinetics and mechanism, J. Environ. Chem. Eng. 5 (2017), https://doi.org/10.1016/j.jece.2017.10.054.

[109] R. Mu, Y. Ao, T. Wu, C. Wang, P. Wang, Synthesis of novel ternary heterogeneous anatase-TiO2 (B) biphase nanowires/Bi4O5I2 composite photocatalysts for the highly efficient degradation of acetaminophen under visible light irradiation, J. Hazard. Mater. 382 (2020), https://doi.org/10.1016/j.jhazmat.2019.121083.

[110] T. Yan, T. Wu, Y. Zhang, M. Sun, X. Wang, Q. Wei, B. Du, Fabrication of In2S3/Zn2GeO4 composite photocatalyst for degradation of acetaminophen under visible light, J. Colloid Interface Sci. 506 (2017), https://doi.org/10.1016/j.jcis.2017.06.079.

[111] X. Wang, M. Brigante, W. Dong, Z. Wu, G. Mailhot, Degradation of Acetaminophen via UVA-induced advanced oxidation processes (AOPs). Involvement of different radical species: HO[rad], SO4[rad]− and HO2[rad]/O2[rad]−, Chemosphere 258 (2020) https://doi.org/10.1016/j.chemosphere.2020.127268.

[112] S. Nezar, N.A. Laoufi, Electron acceptors effect on photocatalytic degradation of metformin under sunlight irradiation, Sol. Energy 164 (2018), https://doi.org/10.1016/j.solener.2018.02.065.

[113] L. Djouadi, H. Khalaf, H. Boukhatem, H. Boutoumi, A. Kezzime, J.A. Santaballa, M. Canle, Degradation of aqueous ketoprofen by heterogeneous photocatalysis using Bi2S3/TiO2–Montmorillonite nanocomposites under simulated solar irradiation, Appl. Clay Sci. 166 (2018), https://doi.org/10.1016/j.clay.2018.09.008.

[114] S. Garcia-Segura, E. Brillas, Applied photoelectrocatalysis on the degradation of organic pollutants in wastewaters, J. Photochem. Photobiol. C. Photochem. Rev. 31 (2017), https://doi.org/10.1016/j.jphotochemrev.2017.01.005.

[115] E. Brillas, A review on the photoelectro-Fenton process as efficient electrochemical advanced oxidation for wastewater remediation. Treatment with UV light, sunlight, and coupling with conventional and other photo-assisted advanced technologies, Chemosphere 250 (2020), 126198, https://doi.org/10.1016/j.chemosphere.2020.126198.

[116] G.G. Bessegato, T.T. Guaraldo, J.F. de Brito, M.F. Brugnera, M.V.B. Zanoni, Achievements and trends in photoelectrocatalysis: from environmental to energy

applications, Electrocatalysis 6 (2015), https://doi.org/10.1007/s12678-015-0259-9.

[117] P. Mazierski, A.F. Borzyszkowska, P. Wilczewska, A. Białk-Bielińska, A. Zaleska-Medynska, E.M. Siedlecka, A. Pieczyńska, Removal of 5-fluorouracil by solar-driven photoelectrocatalytic oxidation using Ti/TiO2(NT) photoelectrodes, Water Res. 157 (2019), https://doi.org/10.1016/j.watres.2019.04.010.

[118] K. Changanaqui, E. Brillas, H. Alarcón, I. Sirés, ZnO/TiO2/Ag2Se nanostructures as photoelectrocatalysts for the degradation of oxytetracycline in water, Electrochim. Acta 331 (2020), https://doi.org/10.1016/j.electacta.2019.135194.

[119] L. Cheng, Y. Tian, J. Zhang, Construction of p-n heterojunction film of Cu2O/α-Fe2O3 for efficiently photoelectrocatalytic degradation of oxytetracycline, J. Colloid Interface Sci. 526 (2018), https://doi.org/10.1016/j.jcis.2018.04.106.

[120] T. Jiang, L. Cheng, Y. Han, J. Feng, J. Zhang, One-pot hydrothermal synthesis of Bi2O3-WO3 p-n heterojunction film for photoelectrocatalytic degradation of norfloxacin, Sep. Purif. Technol. 238 (2020), https://doi.org/10.1016/j.seppur.2019.116428.

[121] M. Jia, Z. Yang, H. Xu, P. Song, W. Xiong, J. Cao, Y. Zhang, Y. Xiang, J. Hu, C. Zhou, Y. Yang, W. Wang, Integrating N and F co-doped TiO2 nanotubes with ZIF-8 as photoelectrode for enhanced photo-electrocatalytic degradation of sulfamethazine, Chem. Eng. J. 388 (2020), 124388, https://doi.org/10.1016/j.cej.2020.124388.

[122] J. Sun, Y. Guo, Y. Wang, D. Cao, S. Tian, K. Xiao, R. Mao, X. Zhao, H2O2 assisted photoelectrocatalytic degradation of diclofenac sodium at g-C3N4/BiVO4 photoanode under visible light irradiation, Chem. Eng. J. 332 (2018), https://doi.org/10.1016/j.cej.2017.09.041.

[123] H.S. Kushwaha, N.A. Madhar, B. Ilahi, P. Thomas, A. Halder, R. Vaish, Efficient solar energy conversion using CaCu3Ti4O12 photoanode for photocatalysis and photoelectrocatalysis, Sci. Rep. 6 (2016), https://doi.org/10.1038/srep18557.

[124] I. Olvera-Rodríguez, R. Hernández, A. Medel, C. Guzmán, L. Escobar-Alarcón, E. Brillas, I. Sirés, K. Esquivel, TiO2/Au/TiO2 multilayer thin-film photoanodes synthesized by pulsed laser deposition for photoelectrochemical degradation of organic pollutants, Sep. Purif. Technol. 224 (2019), https://doi.org/10.1016/j.seppur.2019.05.020.

[125] M. Alvaro, B. Cojocaru, A.A. Ismail, N. Petrea, B. Ferrer, F.A. Harraz, V. I. Parvulescu, H. Garcia, Visible-light photocatalytic activity of gold nanoparticles supported on template-synthesized mesoporous titania for the decontamination of the chemical warfare agent Soman, Appl. Catal. B Environ. 99 (2010) 191–197, https://doi.org/10.1016/J.APCATB.2010.06.019.

[126] S. He, C. Yan, X.Z. Chen, Z. Wang, T. Ouyang, M.L. Guo, Z.Q. Liu, Construction of core-shell heterojunction regulating α-Fe2O3 layer on CeO2 nanotube arrays enables highly efficient Z-scheme photoelectrocatalysis, Appl. Catal. B Environ. 276 (2020), https://doi.org/10.1016/j.apcatb.2020.119138.

[127] H. Du, W. Pu, Y. Wang, K. Yan, J. Feng, J. Zhang, C. Yang, J. Gong, Synthesis of BiVO4/WO3 composite film for highly efficient visible light induced photoelectrocatalytic oxidation of norfloxacin, J. Alloy. Compd. 787 (2019), https://doi.org/10.1016/j.jallcom.2019.01.390.

[128] D. Cao, Y. Wang, M. Qiao, X. Zhao, Enhanced photoelectrocatalytic degradation of norfloxacin by an Ag3PO4/BiVO4 electrode with low bias, J. Catal. 360 (2018), https://doi.org/10.1016/j.jcat.2018.01.017.

[129] V. Cristino, L. Pasti, N. Marchetti, S. Berardi, C.A. Bignozzi, A. Molinari, F. Passabi, S. Caramori, L. Amidani, M. Orlandi, N. Bazzanella, A. Piccioni, J. Kopula Kesavan, F. Boscherini, L. Pasquini, Photoelectrocatalytic degradation of emerging contaminants at WO3/BiVO4 photoanodes in aqueous solution, Photochem. Photobiol. Sci. 18 (2019), https://doi.org/10.1039/c9pp00043g.

[130] K. Wang, G. Liang, M. Waqas, B. Yang, K. Xiao, C. Zhu, J. Zhang, Peroxymonosulfate enhanced photoelectrocatalytic degradation of ofloxacin using an easily coated cathode, Sep. Purif. Technol. 236 (2020), https://doi.org/10.1016/j.seppur.2019.116301.

[131] S. Liu, X. Zhao, H. Zeng, Y. Wang, M. Qiao, W. Guan, Enhancement of photoelectrocatalytic degradation of diclofenac with persulfate activated by Cu cathode, Chem. Eng. J. 320 (2017), https://doi.org/10.1016/j.cej.2017.03.047.

[132] B.O. Orimolade, B.A. Koiki, G.M. Peleyeju, O.A. Arotiba, Visible light driven photoelectrocatalysis on a FTO/BiVO4/BiOI anode for water treatment involving emerging pharmaceutical pollutants, Electrochim. Acta 307 (2019), https://doi.org/10.1016/j.electacta.2019.03.217.

[133] N. Wardenier, Z. Liu, A. Nikiforov, S.W.H. Van Hulle, C. Leys, Micropollutant elimination by O3, UV and plasma-based AOPs: An evaluation of treatment and energy costs, Chemosphere 234 (2019) 715–724, https://doi.org/10.1016/J.CHEMOSPHERE.2019.06.033.

[134] I. Muñoz, J. Peral, J. Antonio Ayllón, S. Malato, M. José Martin, J. Yves Perrot, M. Vincent, X. Domènech, Life-cycle assessment of a coupled advanced oxidation-biological process for wastewater treatment: comparison with granular activated carbon adsorption, Environ. Eng. Sci. 24 (2007) 638–651, https://doi.org/10.1089/ees.2006.0134.

[135] M.J. Lima, C.G. Silva, A.M.T. Silva, J.C.B. Lopes, M.M. Dias, J.L. Faria, Homogeneous and heterogeneous photo-Fenton degradation of antibiotics using an innovative static mixer photoreactor, Chem. Eng. J. 310 (2017), https://doi.org/10.1016/j.cej.2016.04.032.

[136] Q. Li, H. Kong, P. Li, J. Shao, Y. He, Photo-Fenton degradation of amoxicillin via magnetic TiO2-graphene oxide-Fe3O4 composite with a submerged magnetic separation membrane photocatalytic reactor (SMSMPR), J. Hazard. Mater. 373 (2019), https://doi.org/10.1016/j.jhazmat.2019.03.066.

[137] D. Du, W. Shi, L. Wang, J. Zhang, Yolk-shell structured Fe3O4@void@TiO2 as a photo-Fenton-like catalyst for the extremely efficient elimination of tetracycline, Appl. Catal. B Environ. 200 (2017), https://doi.org/10.1016/j.apcatb.2016.07.043.

[138] P. Bansal, A. Verma, In-situ dual effect studies using novel Fe-TiO2 composite for the pilot-plant degradation of pentoxifylline, Chem. Eng. J. 332 (2018) 682–694, https://doi.org/10.1016/j.cej.2017.09.121.

[139] L. Shao, J. Gao, X. Xia, W. Dong, S. Cheng, Y. Zhu, Y. Liu, Solid solution FeNiS: an efficient visible light photo-Fenton catalyst at neutral pH for degradation of organic pollutants, J. Photochem. Photobiol. A Chem. 382 (2019), https://doi.org/10.1016/j.jphotochem.2019.111972.

[140] E.S. Emídio, P. Hammer, R.F.P. Nogueira, Simultaneous degradation of the anticancer drugs 5-fluorouracil and cyclophosphamide using a heterogeneous photo-Fenton process based on copper-containing magnetites (Fe3-xCuxO4), Chemosphere 241 (2020), https://doi.org/10.1016/j.chemosphere.2019.124990.

[141] X.S. Nguyen, G. Zhang, X. Yang, Mesocrystalline Zn-Doped Fe3O4 hollow submicrospheres: formation mechanism and enhanced photo-fenton catalytic performance, ACS Appl. Mater. Interfaces 9 (2017), https://doi.org/10.1021/acsami.6b16839.

[142] F. Velichkova, H. Delmas, C. Julcour, B. Koumanova, Heterogeneous fenton and photo-fenton oxidation for paracetamol removal using iron containing ZSM-5 zeolite as catalyst, AIChE J. 63 (2017), https://doi.org/10.1002/aic.15369.

[143] W. Du, Q. Xu, D. Jin, X. Wang, Y. Shu, L. Kong, X. Hu, Visible-light-induced photo-Fenton process for the facile degradation of metronidazole by Fe/Si codoped TiO2, RSC Adv. 8 (2018), https://doi.org/10.1039/c8ra08114j.

[144] X. Han, S. Liu, X. Huo, F. Cheng, M. Zhang, M. Guo, Facile and large-scale fabrication of (Mg,Ni)(Fe,Al)2O4 heterogeneous photo-Fenton-like catalyst from saprolite laterite ore for effective removal of organic contaminants, J. Hazard. Mater. 392 (2020), https://doi.org/10.1016/j.jhazmat.2020.122295.

[145] L. Guo, K. Zhang, X. Han, Q. Zhao, D. Wang, F. Fu, 2D in-plane CuS/Bi2WO6 p-n heterostructures with promoted visible-light-driven photo-fenton degradation performance, Nanomaterials 9 (2019), https://doi.org/10.3390/nano9081151.

[146] X. Yu, X. Lin, W. Feng, W. Li, Effective removal of tetracycline by using bio-templated synthesis of TiO2/Fe3O4 heterojunctions as a UV–Fenton catalyst, Catal. Lett. 149 (2019), https://doi.org/10.1007/s10562-018-2544-8.

[147] Y. Zhang, J. Zhou, J. Chen, X. Feng, W. Cai, Rapid degradation of tetracycline hydrochloride by heterogeneous photocatalysis coupling persulfate oxidation with MIL-53(Fe) under visible light irradiation, J. Hazard. Mater. 392 (2020), https://doi.org/10.1016/j.jhazmat.2020.122315.

[148] N. Nasseh, B. Barikbin, L. Taghavi, Photocatalytic degradation of tetracycline hydrochloride by FeNi3/SiO2/CuS magnetic nanocomposite under simulated solar irradiation: efficiency, stability, kinetic and pathway study, Environ. Technol. Innov. 20 (2020), https://doi.org/10.1016/j.eti.2020.101035.

[149] S. Stets, B. do Amaral, J.T. Schneider, I.R. de Barros, M.V. de Liz, R.R. Ribeiro, N. Nagata, P. Peralta-Zamora, Antituberculosis drugs degradation by UV-based advanced oxidation processes, J. Photochem. Photobiol. A Chem. 353 (2018), https://doi.org/10.1016/j.jphotochem.2017.11.006.

[150] H. Derikvandi, A. Nezamzadeh-Ejhieh, Comprehensive study on enhanced photocatalytic activity of heterojunction ZnS-NiS/zeolite nanoparticles: experimental design based on response surface methodology (RSM), impedance spectroscopy and GC-MASS studies, J. Colloid Interface Sci. 490 (2017), https://doi.org/10.1016/j.jcis.2016.11.105.

[151] H. Derikvandi, A. Nezamzadeh-Ejhieh, Synergistic effect of p-n heterojunction, supporting and zeolite nanoparticles in enhanced photocatalytic activity of NiO and SnO2, J. Colloid Interface Sci. 490 (2017), https://doi.org/10.1016/j.jcis.2016.11.069.

[152] H. Derikvandi, A. Nezamzadeh-Ejhieh, A comprehensive study on enhancement and optimization of photocatalytic activity of ZnS and SnS2: response surface methodology (RSM), n-n heterojunction, supporting and nanoparticles study, J. Photochem. Photobiol. A Chem. 348 (2017), https://doi.org/10.1016/j.jphotochem.2017.08.007.

[153] J. Trawiński, R. Skibiński, Rapid degradation of clozapine by heterogeneous photocatalysis. Comparison with direct photolysis, kinetics, identification of transformation products and scavenger study, Sci. Total Environ. 665 (2019), https://doi.org/10.1016/j.scitotenv.2019.02.124.

[154] N.L. Finčur, J.B. Krstić, F.S. Šibul, D.V. Šojić, V.N. Despotović, N.D. Banić, J. R. Agbaba, B.F. Abramović, Removal of alprazolam from aqueous solutions by heterogeneous photocatalysis: influencing factors, intermediates, and products, Chem. Eng. J. 307 (2017), https://doi.org/10.1016/j.cej.2016.09.008.

[155] K. Liu, Z. Tong, Y. Muhammad, G. Huang, H. Zhang, Z. Wang, Y. Zhu, R. Tang, Synthesis of sodium dodecyl sulfate modified BiOBr/magnetic bentonite photocatalyst with three-dimensional parterre like structure for the enhanced photodegradation of tetracycline and ciprofloxacin, Chem. Eng. J. 388 (2020), https://doi.org/10.1016/j.cej.2020.124374.

[156] M. Ji, J. Di, Y. Ge, J. Xia, H. Li, 2D–2D stacking of graphene-like g-C3N4 /Ultrathin Bi4O5Br2 with matched energy band structure towards antibiotic removal, Appl. Surf. Sci. 413 (2017), https://doi.org/10.1016/j.apsusc.2017.03.287.

[157] A. Rahmani-Aliabadi, A. Nezamzadeh-Ejhieh, A visible light FeS/Fe2S3/zeolite photocatalyst towards photodegradation of ciprofloxacin, J. Photochem. Photobiol. A Chem. 357 (2018), https://doi.org/10.1016/j.jphotochem.2018.02.006.

[158] H. Wang, J. Li, P. Huo, Y. Yan, Q. Guan, Preparation of Ag2O/Ag2CO3 /MWNTs composite photocatalysts for enhancement of ciprofloxacin degradation, Appl. Surf. Sci. 366 (2016), https://doi.org/10.1016/j.apsusc.2015.12.229.

[159] H. Azizi-Toupkanloo, M. Karimi-Nazarabad, M. Shakeri, M. Eftekhari, Photocatalytic mineralization of hard-degradable morphine by visible light-driven Ag@g-C3N4 nanostructures, Environ. Sci. Pollut. Res. 26 (2019), https://doi.org/10.1007/s11356-019-06274-9.

[160] R. Molinari, C. Lavorato, P. Argurio, Recent progress of photocatalytic membrane reactors in water treatment and in synthesis of organic compounds. A review, Catal. Today 281 (2017), https://doi.org/10.1016/j.cattod.2016.06.047.

[161] G. Gupta, A. Kaur, A.S.K. Sinha, S.K. Kansal, Photocatalytic degradation of levofloxacin in aqueous phase using Ag/AgBr/BiOBr microplates under visible light, Mater. Res. Bull. 88 (2017), https://doi.org/10.1016/j.materresbull.2016.12.016.

[162] J.C. Arévalo-Pérez, D. de la Cruz-Romero, A. Cordero-García, C.E. Lobato-García, A. Aguilar-Elguezabal, J.G. Torres-Torres, Photodegradation of 17 α-methyltestosterone using TiO_2 -Gd^{3+} and TiO_2-Sn^{3+} photocatalysts and simulated solar radiation as an activation source, Chemosphere 249 (2020), https://doi.org/10.1016/j.chemosphere.2020.126497.

[163] X. Yao, X. Hu, Y. Liu, X. Wang, X. Hong, X. Chen, S.C. Pillai, D.D. Dionysiou, D. Wang, Simultaneous photocatalytic degradation of ibuprofen and H_2 evolution over Au/sheaf-like TiO_2 mesocrystals, Chemosphere 261 (2020), https://doi.org/10.1016/j.chemosphere.2020.127759.

[164] V. Kitsiou, G.A. Zachariadis, D.A. Lambropoulou, D. Tsiplakides, I. Poulios, Mineralization of the antineoplastic drug carboplatin by heterogeneous photocatalysis with simultaneous synthesis of platinum-modified TiO_2 catalysts, J. Environ. Chem. Eng. 6 (2018), https://doi.org/10.1016/j.jece.2018.03.036.

[165] G. Gupta, S.K. Kansal, Novel 3-D flower like Bi_3O_4Cl/BiOCl p-n heterojunction nanocomposite for the degradation of levofloxacin drug in aqueous phase, Process Saf. Environ. Prot. 128 (2019), https://doi.org/10.1016/j.psep.2019.06.008.

[166] G. Gupta, A. Umar, A. Kaur, S. Sood, A. Dhir, S.K. Kansal, Solar light driven photocatalytic degradation of ofloxacin based on ultra-thin bismuth molybdenum oxide nanosheets, Mater. Res. Bull. 99 (2018), https://doi.org/10.1016/j.materresbull.2017.11.033.

[167] R. Meribout, Y. Zuo, A.A. Khodja, A. Piram, S. Lebarillier, J. Cheng, C. Wang, P. Wong-Wah-Chung, Photocatalytic degradation of antiepileptic drug carbamazepine with bismuth oxychlorides (BiOCl and BiOCl/AgCl composite) in water: efficiency evaluation and elucidation degradation pathways, J. Photochem. Photobiol. A Chem. 328 (2016), https://doi.org/10.1016/j.jphotochem.2016.04.024.

[168] J. Li, M. Han, Y. Guo, F. Wang, C. Sun, Fabrication of $FeVO_4$/Fe_2TiO_5 composite catalyst and photocatalytic removal of norfloxacin, Chem. Eng. J. 298 (2016), https://doi.org/10.1016/j.cej.2016.03.107.

[169] R. Sabouni, H. Gomaa, Photocatalytic degradation of pharmaceutical micro-pollutants using ZnO, Environ. Sci. Pollut. Res. 26 (2019), https://doi.org/10.1007/s11356-018-4051-2.

[170] S. Sharma, A.O. Ibhadon, M. Grazia Francesconi, S.K. Mehta, S. Elumalai, S. K. Kansal, A. Umar, S. Baskoutas, Bi_2WO_6/C-dots/TiO_2: a novel z-scheme photocatalyst for the degradation of fluoroquinolone levofloxacin from aqueous medium, Nanomaterials 10 (2020), https://doi.org/10.3390/nano10050910.

[171] M. Malakootian, N. Olama, M. Malakootian, A. Nasiri, Photocatalytic degradation of metronidazole from aquatic solution by TiO_2-doped Fe^{3+} nano-photocatalyst, Int. J. Environ. Sci. Technol. 16 (2019), https://doi.org/10.1007/s13762-018-1836-2.

[172] Y. He, C. Dai, X. Zhou, Magnetic cobalt ferrite composite as an efficient catalyst for photocatalytic oxidation of carbamazepine, Environ. Sci. Pollut. Res. 24 (2017), https://doi.org/10.1007/s11356-016-7978-1.

[173] S. Zuo, Y. Chen, W. Liu, C. Yao, X. Li, Z. Li, C. Ni, X. Liu, A facile and novel construction of attapulgite/Cu_2O/Cu/g-C_3N_4 with enhanced photocatalytic activity for antibiotic degradation, Ceram. Int. 43 (2017), https://doi.org/10.1016/j.ceramint.2016.11.173.

[174] B.O. Orimolade, B.N. Zwane, B.A. Koiki, L. Tshwenya, G.M. Peleyeju, N. Mabuba, M. Zhou, O.A. Arotiba, Solar photoelectrocatalytic degradation of ciprofloxacin at a FTO/$BiVO_4$/MnO_2 anode: kinetics, intermediate products and degradation pathway studies, J. Environ. Chem. Eng. 8 (2020), https://doi.org/10.1016/j.jece.2019.103607.

[175] Q. Zeng, J. Li, L. Li, J. Bai, L. Xia, B. Zhou, Synthesis of WO_3/$BiVO_4$ photoanode using a reaction of bismuth nitrate with peroxovanadate on WO_3 film for efficient photoelectrocatalytic water splitting and organic pollutant degradation, Appl. Catal. B Environ. 217 (2017), https://doi.org/10.1016/j.apcatb.2017.05.072.

[176] B.O. Orimolade, O.A. Arotiba, Towards visible light driven photoelectrocatalysis for water treatment: Application of a FTO/$BiVO_4$/Ag_2S heterojunction anode for the removal of emerging pharmaceutical pollutants, Sci. Rep. 10 (2020), https://doi.org/10.1038/s41598-020-62425-w.

[177] Y. Lu, Y. Chu, W. Zheng, M. Huo, H. Huo, J. Qu, H. Yu, Y. Zhao, Significant tetracycline hydrochloride degradation and electricity generation in a visible-light-driven dual photoelectrode photocatalytic fuel cell using $BiVO_4$/TiO_2 NT photoanode and Cu_2O/TiO_2 NT photocathode, Electrochim. Acta 320 (2019), https://doi.org/10.1016/j.electacta.2019.134617.

[178] S. Ghasemian, D. Nasuhoglu, S. Omanovic, V. Yargeau, Photoelectrocatalytic degradation of pharmaceutical carbamazepine using Sb-doped Sn80%-W20%-oxide electrodes, Sep. Purif. Technol. 188 (2017), https://doi.org/10.1016/j.seppur.2017.07.007.